PEOPLE'S DEMOCRATIC REPUBLIC OF ALGERIA

Ministry of High Education and Scientific Research

University of BLIDA1

Institute of Aeronautics and Space Studies

Construction department

A thesis submitted for the Master degree in avionics

Theme:

Elaboration and characterization of Fe-Co based nanocomposites for aircraft coating

Presented by:

SAOU Rania   *KECHTIL Hiba*

Under the supervision of:

M$^{s.}$ OTMANE Fadhela

2019/2020

Acknowledgment

Praise be to ALLAH his majesty for his uncountable blessing and best prayers and peace be unto his best messenger Mohammed, his pure descendent, and his family and his noble companions.

First, it is a great pleasure to acknowledge our sincere gratitude to our dear promoter Ms. «Othman Fadhela» for her patience, motivation, enthusiasm follow-up and her enormous support in which she has constantly guided us throughout the period of our project.

We also would like to express our deepest thanks and appreciation to the jury members for their willingness to examine and judge this work.

Finally, we extend our sincere thanks to our teachers, and to all those who contributed, directly or indirectly, to the smooth running of our project and the success of our university career.

Dedication

In the Name of Allah, the Most Merciful, and Prayers and peace be upon Mohamed His servant and messenger.

I dedicate my dissertation work to my family and many friends. A special feeling of gratitude to my loving parents, **AHMED** and **TADJ NAIMA** whose words of encouragement and push for tenacity ring in my ears, without you none of my accomplishments would turn to reality.

My special sisters **KATR ENNADA, AYA** and **GHINA** that have never left my side making the process way easier. I also dedicate this dissertation wholeheartedly to my second family **KASSIMI** specially the amazing couple **MILOUD** and **FATIMA** who have been there for me through the bitter and sweet, thank you for every thought and every gesture you made because without you none of this would be possible and the **TADJ** family for their generous support they provided me throughout my entire life and particularly through the process of pursuing the master degree. Because of their unconditional love and prayers, I have the chance to complete this thesis

To my beloved friends that I had the chance to know in these past few years of college, I will always appreciate all they have done. Especially **AKRAM** and **MOLOD** for always being there for me and helping me develop my programming skills, my partner **SAOU RANIA** for the many hours of proofreading and the amazing moments we shared in the process.

I dedicate this work and give special thanks to my best friends **LAMIS** and **LIZA**, my dearest friends **RAZIQA**, **LOUIZA**, **AMIR** and **ELIAS** for being there for me throughout my entire college experience.. All of you have been my best cheerleaders, with a very special thanks to the girl who put so much effort in guiding me, correction my errors and being there whenever is needed **FARIDA**.

To all the people in my life who touch my heart, I dedicate this research.

"KECHTIL Hiba"

Dedication

First I would like to thank our God for providing me the ability and the strength that was needed to complete this work.

To whom I owe what I am,

To my dear mother «Hakima» and my dear father «Mohammed», No dedication can be fairly enough to express what you deserve for all the sacrifices you have given me since my birth, during my childhood and even in adulthood, Nothing in the world is worth the efforts made day and night for my education and well-being, your prayers have been of great help to me to carry out my studies and this journey would not have been possible without you.

To my source of joy, my sisters «Maissa», «Dounya» and «Sarah», and my beloved aunt «Fatima» and all «SAOU » members, I dedicate this work whose pleasure is yours for your love, help and your encouragement.

In memory of my grandparents «Djohar» and «Said» I would have liked so much for you to be present, for God to have your souls in his holy mercy.

Special thanks will be given to my dear partner and friend "Kechtil Hiba" for her hard work and support during the making of this study without forgetting the "KECHTIL" family

A special thanks to a very special person who has been my source of strength and courage.

I would like to thank my second family my friends: Yassmine, Imene, Sandra, Amina, Elias, mouloud and Amir for their presence during my university career.

Last but not least I'd like to thank my friends and teachers: Rabea, Selma, Assia and aicha for all their advices and guidance.

"SAOU Rania"

Figures List

Chapter I:

Chapter II:

Chapter III:

Chapter IV:

Tables List

Chapter I:

Chapter II:

Symbols List

Greek letters:

θ: is the diffraction angle.

β: integral breadths

β-sample: the reduced (normalized) integral breadth

2θ: the angle of Bragg (diffraction)

λ: the wavelength of X-ray radiation (A)

ε: micro deformation percentage

σ: conductivity (s.m^{-1})

ε : complex electrical permittivity

εr : relative permittivity

ε_0: vacuum permittivity

ε 'and ε'': real and imaginary components

μ : magnetic permeability

μ'and μ'': real and imaginary components

δ : phase delay

Γ : reflection coefficient

γ: propagation constant

tanδ_E: dielectric loss tangent

$\tan\delta_M$: magnetic loss tangent

Latin letters:

E: kinetic energy

m: the mass

v: the relative velocity

n: an integer

d: is the interplanar spacing generating the diffraction

C: capacitance

J: current density

D: electric flux density

x' and *x''*: real and imaginary components

x: electrical susceptibility

B: magnetic flux density

H: magnetic intensity

d*: reticular distance of the reduced reciprocal system (distance between two crystallographic planes)

a :lattice parameter

(h, k, l): Miller indices corresponding to the diffracting planes.

T : phase factor

k : wave number of the filled waveguide

k_c : cut-off wave number

m and n: half wave length on the a and b sides respectively.

f: frequency

Z_0 and Z_1: transmission line's characteristic impedances in absence and in the presence of the sample respectively

k0: propagation constant in free space

kt: cutoff wave number of the waveguide

Abbreviations List

Al: atom of aluminum

NI: atom of nickel

TBC: Thermal barrier coatings

Sol gel: solution gelefication

SWNT: Single-wall carbon nanotube

MWNT: Multi-Wall Nanotubes

c-MWNT: centric Multi-Wall Nanotubes

MA: mechanical Alloying

MM: mechanical milling

BPR: ball to powder ration

CR: charge ratio

PCA: process control agent

XRD: X-ray diffraction

WH: Williamson–Hall

HW: Halder–Wagner

TEM: Transmission electron microscopy

CTEM: Conventional transmission electron microscopy

STEM: Scanning transmission electron microscopy

SEM: Scanning electronmicroscopy

RF: radio frequency

VHF: very high frequency

UHF:ultra-high frequency

VNA: Vector Network Analyzer

E-field: electric field

MUT: material under test

EM: electromagnetic

TE: transverse electric

TM: transverse magnetic

S-parameters: scattering parameters

RFA: Root Find Algorithm

GA: Genetic Algorithm

Rpm: rounds per minute

Bcc: Bravais crystalline cubic

Fe: atom of iron

Co: atom of cobalt

Abstract

This dissertation is devoted to study the elaboration, structural and electromagnetic characterization of Fe-Co based nanocomposites for aircraft nanocoatings. After a general state of the art on nanomaterials in aircraft coatings, elaboration and structural characterization methods are approached. A particular interest is focused on the interaction between material's medium and microwaves and the available methods to investigate this interaction (electromagnetic characterization methods). As application Fe-Co based nanocomposites are elaborated via the mechanical alloying process. Structural characterization is conducted using the Halder-Wagner theory (X-Ray Diffraction analysis) and Scanning Electron Microscopy. Finally, electromagnetic characterization is conducted in a metallic wave-guide associated to a VNA over the microwave X-band (8.2-12.4 GHz).

Résumé

Ce travail est consacré à l'étude de l'élaboration, caractérisation structurelle et électromagnétique de Nanocomposites à base de Fe-Co pour les nanocoatings d'avions. Après un état de l'art général des nanomatériaux dans les revêtements avion, des méthodes d'élaboration et de caractérisation structurale sont abordées. Un intérêt particulier est porté sur l'interaction entre le milieu du matériau, les micro-ondes et les méthodes disponibles pour étudier cette interaction (méthodes de caractérisation électromagnétique). Comme application, des Nanocomposites à base de Fe-Co sont élaborés via le processus d'alliage mécanique. La caractérisation structurelle est réalisée à l'aide de la théorie de Halder-Wagner (analyse de diffraction des rayons X) et de la microscopie électronique à balayage. Enfin, la caractérisation électromagnétique est effectuée dans un guide d'ondes métallique associé à un VNA sur la bande X des hyperfréquences (8,2-12,4 GHz).

ملخص

هذه الاطروحة مكرسة لدراسة الخصائص التركيبية والكهرومغناطيسية لعينات نانو مركبة ومكونة اساسا من الحديد والكوبالت كمادة مستخدمة في مجال طلاء الطائرات وبعد ان اصبحتالمواد النانومترية في طلاء الطائرات متطورة يتم مناقشة اساليب و طرق الصياغة و المعاينة التركيبية. يركز الاهتمام في هذه الاطروحة على العلاقة بين وسط المادة و الميكروويف و الطرق المتاحة لدراسة هذا التفاعل (طرق المعاينة الكهرومغناطيسية). كتطبيق استخدام طريقة المزج المعدني الميكانيكي للحصول على مركب الحديد و الكوبالت النانومتري. نظرية هالدر- واغنر و مسح المجهر الالكتروني تسمح بإجراء التشخيص التركيبي و الهيكلي لهذه المادة و في الاخير تم الحصول على الخصائص الكهرومغناطيسية للعينات المعرضة لحقل كهرومغناطيسي ضمن مسار موجي حديدي موصول ب محللشبكات موجه لمجال ترددات اكس(GHz 8,2-12,4).

Contents

Chapter II: Microwave and material mediums

Chapter III: structural characterization and results

Chapter IV: Electromagnetic characterization and results

General Introduction

Aeronautical Science is the specialization that underlies the study, design, and manufacture of aircrafts. One of the three most important factors affecting the efficiency of an aircraft after aerodynamics and engine performance is weight. Building lighter aircrafts is very beneficial for the industry and the aircraft operators, as it can result in more fuel savings, which means lower carbon dioxide emissions, as well as savings on a significant operating cost, and longer aircraft ranges for airlines. One of the solutions consists in aircraft coating.

Currently under development, there are multifunctional nanocoatings for aerospace that can present not only lighter aircraft but also corrosion protection using environmentally safe materials with many types of design models for nanostructured coatings, such as nanocomposites coatings.

Nanocomposites are finding applications in engine components and fuel storage due to their increased lifetime, enhanced strength, elastic modulus and improved polymer barrier properties. Other nanomaterials have a great potential in aerospace components for comfort and safety, control of air quality and noise reduction.

Optimizing coating properties requires understanding the complex relationships between coating structure and the different material properties. For example, the structural properties of nanocomposites are investigated using the X-Ray Diffraction Technique (XRD) and the Scanning Electron Microscopy (SEM). The electromagnetic properties of materials are defined by two

parameters: the relative permittivity that reflects the comportment of the material to an electric excitation (electromagnetic wave E field) and relative permeability, which describes the behavior of the material towards a magnetic excitation (electromagnetic wave H field). The relative dielectric permittivity and magnetic permeability are represented by complex values to account for dissipative effects (losses) inherent in any material environment. With the advance of new technologies, a vector network analyzer can be employed to measure the complex transmission/reflection coefficients and a software program converts the data into the complex dielectric property parameter.

In this context, our work is committed to the study of the structural properties of Fe-Co based nanocomposites at different elaboration times. An electromagnetic characterization is also conducted in order to show the behavior of particular samples when exposed to the action of an electromagnetic field in an X-band rectangular waveguide, for this, we have structured this work in the following points:

- First chapter is devoted to a bibliographic study of aircraft coatings and the evolution of nanocomposites use and the different nanomaterials elaboration methods established.
- Second chapter is dedicated to the electromagnetic characterization: a description of the electromagnetic properties (permittivity and permeability) and the methodologies that can accurately characterize these properties of materials. We established also the NRW (Nicholson Ross weir) extraction method to obtain the electromagnetic properties.
- In the third chapter, we described the elaboration and characterization processes and the structural calculation conducted for the test samples.
- In the fourth chapter, we present some electromagnetic characterization results to show the advantages of nanocomposites.

Finally, a general conclusion with future prospects to sum our work.

Chapter I: aircraft coating

- **Introduction**

Coatings in aircraft industry are required to provide improvements to engine efficiency and longevity. Although they are not a new technology, aircraft coatings are being continuously improved (new materials, old modified methods) to meet new requirements. Optimizing coating properties require understanding the complex relationships between deposition parameters and coating structure. Different coating technologies exist for aircraft applications[1]:

- Super alloys for Aircraft Engines:alloysthat are superior in heat and corrosion resistance. Super alloys generally used above 540^0C; maintain superior properties even at elevated temperatures (synonymous with "high-temperature alloys").They are based on iron, nickel and cobalt.

- Thermal barrier coatings (TBCs): advanced materials systems usually applied to metallic surfaces operating at elevated temperature such as gas turbine or aero engines.

- Abradable seal coatings**:** Generally, a mixture of a metallic or ceramic base material mixed with solid lubricants, used in the compressor and turbine sections.

- Abradable coating materials:Metals (e.g., Al, Ni) mixed with graphite for lower temperatures (compressor turbine) or Ceramic oxides or superalloys mixed with boron nitride for higher temperatures (combustion section).

I.1 State of the Art of aircraft nanocoatings

Nanotechnologies are regarded world- wide as key technologies of the 21[st]century. In aerospace, a high potential for nanotechnological applications is postulated. These technologies could contribute significantly to solutions and technological breakthroughs in this area. Revolutionary solutions can be found within advanced nanomaterials like nanoporous membranes, high strength nanocomposites or adaptive and actuating nanostructures.

All these opportunities will be possible if the following challenges can be overcome:

- Technical challenges: the manipulation and observation of nanosized materials/ systems is not obvious. Reliability, reproducibility, etc… need to be addressed to obtain real products,

- Regulations and standards have to be considered,

- Cost and quantities have to be studied while these materials are under development.

Nanomaterials present an opportunity to deliver unprecedented material performance. This opportunity is based on the original properties (mechanical, thermal, electric, magnetic...) that vary with changes in the material's size at the nanoscale (1- 10 nm). Working at the nanoscale offers the possibility to create materials with functions and properties needed to solve specific problems.

Opportunities presented by nanomaterials have been widely documented. Real problems and applications can be addressed with this new perspective on the design of novel materials that could revolutionize the aerospace sector. Currently under development, there are multifunctional nanocoatings for aerospace that can provide corrosion protection using environmentally safe materials, sense corrosion and mechanical damage of aircraft skin, initiate responses to sensed damage either as alarm changes in colour or real self-healing behaviours, and improve fatigue resistance [2]. There are many types of design models for nanostructured coatings, such as nanocomposites coatings, nano-scale multilayer coatings, superlattice coatings, nano-graded coatings, etc [3, 4, 5]. For moving parts, new aspect of the nanocoatings comes with new compositions like crystalline carbides, diamond- like carbon and metal dichanogenides for wear- resistant and low friction applications [6, 7, 8, 9].Nanostructured layers deposited via thermal spraying are developed. High temperatures of operation were also reported for nanocoatings with various porosities [10, 11]. Other applications that can be considered are the introduction of new functionalities like anti-scratch, anti- strain, self- repairing and specially the ability to introduce several of them in the same nanocoating without losing most of the required properties. Nanocomposites based on various metal, ceramic or plastic matrix material strengthened by metal or ceramic nanoparticles or nanoplatelets can also improve the strength by 100%. In this context, layered silicate nanocomposites are finding applications in engine components and fuel storage due to their increased lifetime, enhanced strength and elastic modulus and improved polymer barrier properties. Other nanomaterials have a great potential in aerospace components, such as nanoporous filters for comfort and safety, control of air quality and noise reduction.

I.2 Nanocompositescoatings

A composite is a combination of two or more different materials that are mixed in an effort to blend the best properties of both. It consists of an assemblage of materials of different natures allowing us to obtain a material of which the set of performance characteristics is greater than that of the components taken separately.

The term nanocomposite is adequately used to describe an extremely broad range of materials, where one of the dimensions is in nano scale. Nanocomposites are composed of two or more distinct constituents or phases having different physical and chemical properties and are separated by a distinct interface. Their unique properties are not depicted by any of the constituents. The constituent that is generally present in greater quantity is called the matrix. The constituent that is embedded into the matrix material in order to improve the mechanical properties of nanocomposites is called reinforcement. Reinforcement is generally in the form of nanosized filler materials. Generally, nanocomposites show anisotropy (properties are directionally dependent) because of the distinct properties of constituents and inhomogeneous distribution of the reinforcement.

I.2.1 Definition

A nanocomposite coating is a material composed of at least two immiscible phases, separated from one another by interface region. The material must contain the nanometer scale in at least one dimension in which the major component is called matrix in which fillers are dispersed.

I.2.2 Classification

The classification of nanocomposite coatings is based on various methods dealing with:

- Type of nanostructured fillers
- Type of matrix where filler nanostructures are dispersed.

I.2.3 Types of nanostructured fillers

There are three main groups of nanocomposite coating as follows:

I.2.3.1 0-Dnanocomposite coatings

The fillers are nanoparticles (3 dimensions in nanometer scale).Nanoparticles is generally defined as particulate matter with at least one dimension that is less than 100 nm. This definition puts them in a similar size domain as that of ultrafine particles (airborne/suspended particulates) and places them as a sub-set of colloidal particles (intermediate size between soluble particles and airborne particles). Nanoparticles are in fact complex mixtures. Nanoparticles can be split into two or three layers [12]:

- A surface that may often be functionalized with a range of metal ions, small molecules, surfactants or polymers.

- A shell material that may be intentionally added. The term shell is usually applied to a second layer that has a completely different structure from that of the core material as opposed to a serendipitous variation in chemistry due to being at the top layer of the particle.

- A core material, which is the part of the nanoparticles that results in key properties for most applications. It is essentially the center of the nanoparticles.

Nanoparticles are mainly classified into two groups [13]:

- Organic nanoparticles: commonly described as solid particles composed of organic compounds (mainly lipids or polymeric) ranging in diameter from 10 nm to 1μm.

- Inorganic nanoparticles: they have certain physical properties that mainly include size-dependent optical, magnetic, electronic, and catalytic properties.

The behavior of nanoparticles is closely related to their intrinsic properties such as mobility, surface energy and colloid stabilization, optical and catalysis.

I.2.3.2 1-Dnanocomposite coatings

The fillers are nanotubesor whiskers (2dimensions in nanometer scale). Carbon nanotubes represent one of the best examples of novel nanostructures derived by bottom-up chemical synthesis approaches. Nanotubes have a simplest chemical composition and atomic bonding

configuration and exhibit an extreme diversity and richness among nanomaterials in structures and structure-property relations. There are two types of carbon nanotubes [14]:

- Single-wall carbon nanotubes (SWNT) that are new nano-objects with properties and behaviors that is often quite specific. It is enough to consider a perfect grapheme sheet (grapheme is a polyaromatic monoatomic layer consisting of sp2-hybridized carbon atoms arranged in hexagons) and to roll it into a cylinder making sure that the hexagonal rings placed in contact join coherently. Then, two caps seal the tube's tips each cap being a hemi-fullerene of the appropriate diameter led to the discovery of single-wall carbon nanotubes (SWNTs).

- Multiwall Nanotubes in which (the concentric type: c-MWNT) SWNTs with regularly increasing diameters are coaxially arranged into a multiwall nanotubes. It can have any number of walls (or coaxial tubes), from two upwards.

Metallic and semiconducting nanotubes exist in all materials synthesized by arc-discharge, laser ablation, and chemical vapor deposition methods. The properties of carbon nanotubes depend on whether they are arranged as SWNTs or as MWNTs.

I.2.3.3 2-Dnanocomposite coatings

The fillers are nanolayers (1 dimension in nanometer scale). In this context, surface's coatings based on elementary nanolayers or multilayers are considered. The application of graphene has been gained increasing attention by researchers because of its original properties [15].
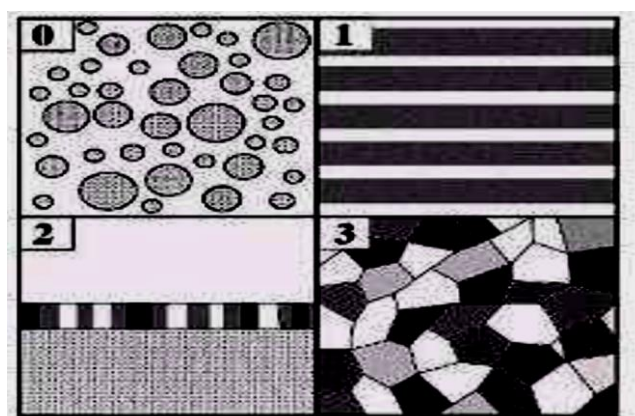
Figure I.1 : Nanomaterials categories.

(0): ultrafine powders, (1): nanofils and nanotubes, (2): nanolayers, (3): nanocomposites

I.2.4 Types of matrix:

Two types of matrix, which are organic and inorganic matrix, can be found. Consequently, there are four main groups of nanocomposite coatings as follows (matrix/ nanofiller):

- Organic/inorganic nanocomposite coatings (O/I nanocomposite coatings)
- Organic/organic nanocomposite coatings (O/O nanocomposite coatings)
- Inorganic/organic nanocomposite coatings (I/O nanocomposite coatings)
- Inorganic/inorganic nanocomposite coatings (I/I nanocomposite coatings).

I.2.5 Preparative methods

Several methods are involved in the preparation of the nanocomposite coatings (table I.1).

In this paragraph, we just trace an overview of these methods:

- Sol- gel method for high quality films,
- Thermal spray method often used to make nanocomposite coatings with a metal or alloy matrices,
- Solution dispersion method mainly applied for the preparation of polymer nanocomposite coatings reinforced with nanofillers such as metal oxides, nanoclay and carbon nanotubes.

TABLE 1: Summary of materials, preparative methods, and applications for nanocomposite coatings.

Matrix	Nanofillers	Preparative method	Application	Reference
Organic/inorganic nanocomposite coatings				
Epoxy resin	Oxides, clay	Ultrasonic stirring, solution dispersion	Anticorrosion	[4–7]
Polyester	Clay	Electrostatic method	Anticorrosion Aniwear	[35]
Perfluoroacrylic polymer	ZnO	Spray atomization	Superoleophobic	[29]
Fluoropolymer	CNT, graphene	Drop casting suspensions	Superhydrophobic	[30]
Pullulan	Clay	Ultrasound-assisted	High oxygen barrier	[28]
PAni	Clay	Electrodeposition	Anticorrosion	[19]
Fluorinated polysiloxane	TiO_2	Blending ambient-cured	Superhydrophobic self-cleaning	[34]
Ethylene tetrafluoroethylene	PANi/CNT	Ultrasonic stirring, air spray	Self-cleaning, antiwear, anticorrosion	[31]
Polydimethylsiloxane	SiO_2	Ultrasonic stirring, brushing	Superhydrophobic	[38]
Polydimethylsiloxane	Al_2O_3/Clay	Ultrasonic stirring, spraying	Superhydrophobic	[149]
Polymers with reactive trimethoxysilyl groups	SiO_2	Ultrasonic stirring, spin coating/dip coating	Superhydrophilic	[26]
Polyacrylate	SiO_2	Dip coating	Superhydrophobic and oleophobic	[107]
Epoxy resin	ZnO/PANi	Dip coating	Antifouling and antibacterial	[150]
Polycarbonate	CNT	Ultrasonic stirring, casting	Infrared sensor	[33]
Poly(3-hydroxy-2,3-dimethylacrylic acid)	TiO_2	Spin coater	Color filters for liquid crystal displays	[148]
Polyvinyl alcohol	ZnO	Sol-gel	Biosensor	[37]
Polyvinylidene Fluoride	Au	Ultrasonic stirring, spin coating	dielectric	[16]
Hexafluoroacetylacetonate precursor	Pt	Plasma chemical deposition	Ion- and electron-conducting	[91]
Monomers (N-isopropylacrylamide and/or dodecyl methacrylate)	SiO_2	Evaporation-induced self-assembly, dip coating	Environmentally responsive coatings	[151]
Organic/organic nanocomposite coatings				
PANi	Nanocellulose	In situ polymerization	Electrochromic	[152]
Inorganic/inorganic nanocomposite coatings				
Ni–P	Al_2O_3	Electroless deposition	Anticorrosion Ani-wear	[116, 117]
Co	CeO_2	Electrodeposition	Anticorrosion	[122]
Ni	TiO_2	Electrodeposition	Anticorrosion	[118]
Ni, Cu	TiN, ZrN, ZrN, CrN	Magnetron cosputtering	Superhard	[73–77, 153]
Diamond-like carbon	TiC	Laser-assisted deposition	Superhard	[103, 154]
Diamond-like carbon	TiCrCN	Magnetron sputtering	Superhard	[93]
Si_3N_4	TiN	PVD	Superhard	[155, 156]
Inorganic/organic nanocomposite coatings				
Ni–P	PTFE	Electroless deposition	Anticorrosion Ani-wear	[81]
Ni–P	PTFE	Electroless deposition	Antibiofouling	[82]

TableI.1: Summary of materials, methods and application for nanocomposite coatings.

I.3. Polymer-basednanocomposites

A Polymer-based nanocomposite consists of polymer or copolymer having nanofillers dispersed in the polymer matrix. It can be fabricated either by chemical or mechanical process. Uniform and homogeneous dispersion of nanoparticles in the polymer matrix is one of the major problems encountered in polymer nanocomposite fabrication. The Nanofillers have a tendency to aggregate and form micron size filler cluster, which limit the dispersion of nanoparticles in the polymer matrix thereby deteriorating the properties of nanocomposites. Researchers have made many attempts to disperse nanofillers uniformly and homogeneously in the polymer matrix by chemical reactions, complicated polymerization reactions or surface modification of filler materials. For better dispersion of the nanofillers in the polymer matrices, ultrasound assisted stirring has to be used. Mostly polymer nanocomposites can be fabricated by the following four methods: Intercalation method, in situ polymerization, Sol Gel method, directs Mixing of polymer and Nanofillers (solution dispersion method) [16].

I.4 Nanomaterials elaboration

In nanomaterials discipline we are dealing with very fine structures: a nanometer is a billionth of a meter. This indeed allows to think in both the 'bottom up' or the 'top down' approaches to synthesize nanomaterials which means either to assemble atoms together or to dis-assemble (break, or dissociate) bulk solids into finer pieces until they are constituted of only a few atoms.

I.4.1 Bottom-up approach

This approach includes the miniaturization of materials components (up to atomic level) with further self-assembly process leading to the formation of nanostructures. The bottom-up approach starts with atoms or molecules and builds up to nanostructures. Bottom up processes are lessexpensive.

I.4.2 Top-down approach

This approach uses larger assembly of nanostructures. Typical examples are etching through the mask, ball milling, and application of severe plastic deformation. The top-down process leads to smaller particles mainly by mechanical milling. Consequently, the top-down approach begins with a pattern generated on a larger scale, then reduced to nanoscale. Top-

down techniques are not cheap, quick to manufacture, slow and not suitable for large-scaleproduction.

A second classification of nanomaterials elaboration methods is established as follows:

- **Physical methods:** include laser ablation, sputtering, evaporation condensation in an inert or reactive gas.

- **Chemical methods:** In this route, we have thesol-gel process, the intercalation – reaction synthesis and the co-precipitation- reduction reaction.

- **Mechanical methods:**comprise severe plastic deformation (mechanical alloying, ball milling) and turbulent brewing.

I.5 Mechanical Alloying Technique

The ball milling is the generic term used to denote processing of metal powders in high-energy ball mills. It is a mechanical process able to introduce important severe plastic deformations compared to other mechanical processes. If powders of pure elements A and B (elemental powders) are milled together to synthesize a homogeneous alloy phase, the process is referred to as mechanical Alloying (MA). Material transfer is involved in this process to obtain a homogeneous alloy. When powders of uniform (often-stoichiometric) composition, such as pure metals, inter-metallic, or pre-alloyed powders, are milled in a high-energy ball mill, and material transfer is not required for homogenization, the process has been termed mechanical milling (MM). Only reduction in particleor grain size and increase in the surface area are involved in this process and material transfer does not occur.

During mechanical milling, powder's particles are subject to severe mechanical deformations and repeatedly fractured and welded (Fig.1). This process induces material defects (dislocations/ two-dimensional defects) that lead to the refinement of the grain size and/ or packages of nano-metric defects. The nano- crystallization phenomenology can be supposed to happen in three steps:

- Deformation location of shear bands containing a high density of dislocations,
- A self-gathering of the dislocations collections,

- Random grain rotation due to the rotation of the grain boundaries.
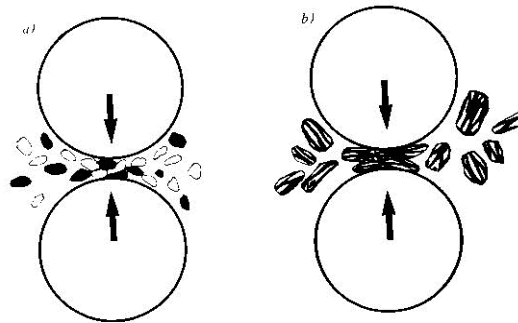
Figure I.2: Fracture- welding mechanisms during MA.

Generated dislocations and other defects act as diffusion paths. Refinement of particles and grain size reduces the diffusion distances. Further, the temperature of powders rises. All these effects lead to alloying of the blended elemental powders during the milling process. Mechanical alloying process starts with mixing elemental powders in the right proportion and loading the powder mix into the mill along with the grinding medium (generally steel balls). This mix is then milled for the desired time duration until a steady state is reached when the composition of every powder particle is the same as the proportion of the elements in the starting powder mix. The milled powder is then consolidated into a bulk shape or heat treated to obtain the desired microstructure and properties. Thus, the important components of the MA process are the raw materials, the mill, and the process variables.

Mechanical alloying is a complex process and hence involves optimization of anumber of variables to achieve the desired product phase and/or microstructure. Some of the important parameters that have an effect on the final constitution ofthe milled powders are:

- **Types of mills:** Different types of high-energy milling equipment are used to produce mechanically alloyed/milled powders. They differ in their design, capacity, efficiency of milling, and additional arrangements for cooling, heating, and so forth.
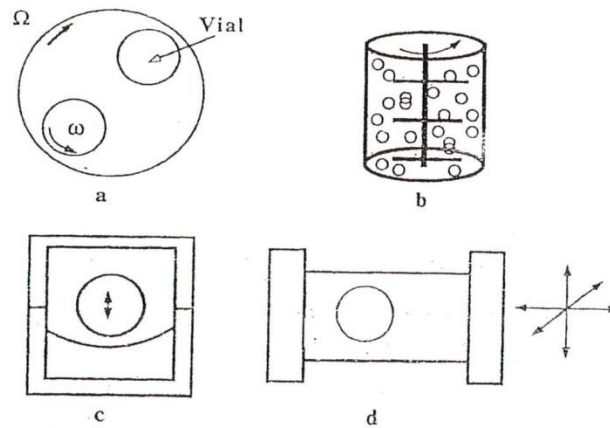
Figure I.3: types of Mills.

(a): planetary, (b): attrition, (c et d): vibration.

Several new designs of mills have been developed in recent years for specialized purposes. These include the rod mills, vibrating frame mills, and others.

- **Milling container:** can contaminate the powder and/or alter the chemistry of the milled powder. The shape of the container (flat-ended and round-endedcontainers) also seems to be important, especially the internal design of the container.

- **Milling energy/speed:** It is easy to realize that the faster the mill rotates the higher will be the energy input into the powder. However, depending on the design of the mill there are certain limitations to the maximal speed that could be employed.Another limitation to the maximal speed is that at high speeds (or intensity of milling) the temperature of the vial may reach a high value. This may be advantageous in some cases may be a disadvantage in others.

- **Milling duration:** The times required vary depending on the type of mill used, mill settings, intensity of milling, ball to powder ration (BPR), and temperature of milling.

- **Grinding medium:** The material of the grinding medium is an important variable. The higher the density of the grinding medium, the more kinetic energy it acquires during milling and this can be transferred to the powder.

- **Ball-to-powder weight ratio:** Generally, the higher the BPR, the faster is the MA process. However, this faster processing also can introduce high contamination levels into the powder, and this should be avoided or at least minimized.

- **Extent of filling the vial:** The extent of filling the vial with the powder and the balls is important. If the quantity of the balls and the powder is very small, then the production rate is very low. On the other hand, if the quantity is large, then there is not enough space for the balls to move around and so the energy of the impact is less. Consequently, alloying may not occur, and even if it occurs, it may take a very long time. About 50% or a little more of the vial space must be left empty.

- **Milling atmosphere:** The major effect of the milling atmosphere is on the nature and extent of contamination of the powder.

- **Milling temperature:** Since diffusion processes are involved in the formation of alloy phases, it is expected that the temperature of milling will have a significant effect in any alloy system.

I.6 Characterization Techniques

I.6.1 X- Ray Diffraction Technique

X-ray diffraction (XRD) is a powerful technique for characterizing crystalline materials. It provides information on structures, phases, preferred crystal orientations (texture), and other structural parameters, such as average grain size, crystallinity, strain, and crystal defects. The atomic planes of a crystal cause an incident beam of X-rays to interfere with one another as they leave the crystal. The phenomenon is called X-ray diffraction. There are several advantages of XRD techniques in science laboratories:

- Nondestructive, fast, and easy sample preparation
- High-accuracy for d-spacing calculations
- Can be done in situ
- Allows characterizing single crystal, poly, and amorphous materials
- Standards are available for thousands of material systems

I.6.1.1 X- Ray Diffraction Instrumentation

The instrumentation used for powder diffraction measurements has not changed much from that developed in the late 1940s. The major difference found in modern instrumentation is the use of the minicomputer for control, data acquisition, and data processing. X-ray diffractometer consists of three basic elements:

- X-ray tube,
- sample holder,
- X-ray detector.

The geometry of an X-ray diffractometer is such that the sample rotates in the path of the collimated X-ray beam at an angle θ while the X-ray detector is mounted on an arm to collect the diffracted X-rays and rotates at an angle of 2θ. The instrument used to maintain the angle and rotate the sample is termed a goniometer. For typical powder patterns, data are collected at 2θ from 5 to 70 angles that are present in the X-ray scan. X-ray powder diffraction is most widely used for the identification of unknown crystalline materials (e.g., minerals, inorganic compounds). Determination of unknown solids is critical to studies in geology, environmental science, material science, engineering, and biology. Other applications include characterization of crystalline materials, identification of fine-grained minerals such as clays and mixed layer clays that are difficult to determine optically, determination of unit cell dimensions, and measurement of sample purity with specialized technique.
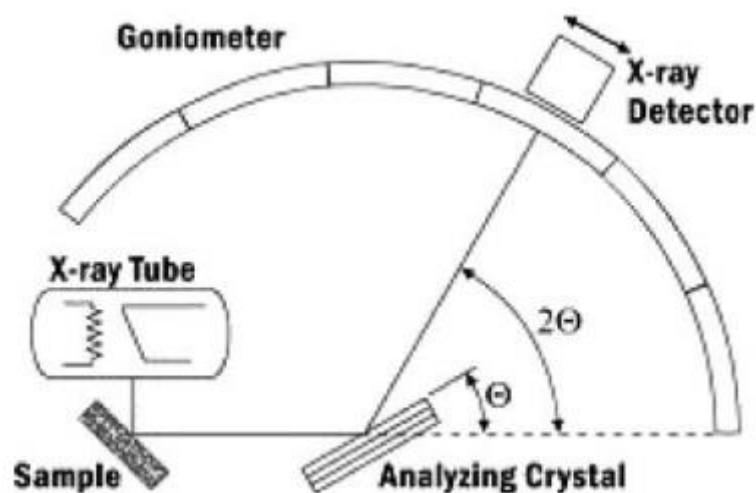
Figure I.4: schematic diagram of a diffractometer system.

I.6.1.2 X- Ray Diffraction Analysis

Analysis of X-ray diffraction spectra on elementary and ground powders allows the following structural parameters to be determined:

- **Structure type:**

Solid materials can be crystals with orderly arrangement of their constituents or amorphous solids that have no such arrangement. Crystalline structure is an arrangement of atoms or groups of atoms in a crystalline solid. The crystalline network is defined by a set of points, which form the nodes of the network, occupied or not by atoms. The localization of nodes is determined by a vector system. Planes of atoms are spaced a distance d apart and can be resolved into many atomic planes, each with a different d spacing. The atoms contained in an elemental mesh form the pattern of a crystal.

Iron can exist in two crystalline forms: the centered cubic form and the centered-faced cubic form. The two forms belong to the cubic system.

- Centered cubic system

In this system, there is one atom in each point of the network and one additional atom in the center of the cube. Fig I.5 represents an elementary cell: the black dots surrounded by a blue circle represent the nodes of the network while the dark blue circles represent the pattern of the cubic mesh.
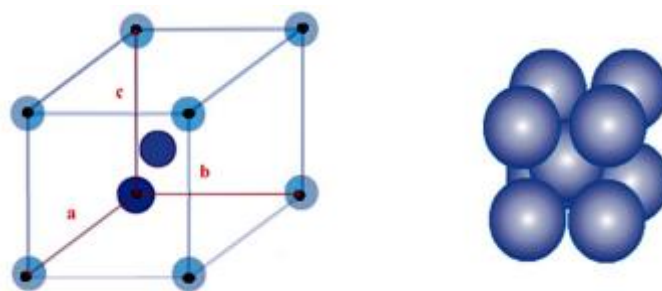
Figure I.5: Centered cubic crystal structure

- Face centered cubic system

For this system, one atom is in each point of the network and each face has an atom in its center. The following figure represents an elementary cell: the black dots surrounded by a blue circle represent the nodes of the network and the dark blue ones represent the pattern of the cubic mesh.
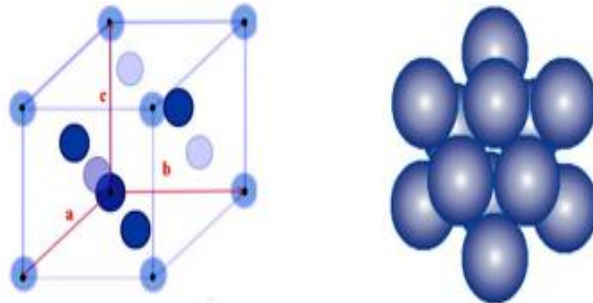
Figure I.6: face centered cubic crystal structure

Iron is centered cubic system between 1394 and 1538 °C temperature, face centered cubic system between 912 and 1394 °C temperature and again centered cubic system for temperatures below 912 °C .

- **Lattice Parameter**

The lattice parameter refers to the physical dimensions of unit cell in a crystal lattice. Lattices in three dimensions generally have three constants referred to as a, b and c. However in the case of cubic crystal structures, all of the constants are equal and are referred to as a.The lattice parameter is evaluated via the Bragg relation:

$$2d_{hkl} sin\theta = \lambda \qquad (1)$$

With,

$$d_{hkl} = \frac{a}{\sqrt{h^2 + k^2 + l^2}}$$

Which leads to :

$$a = \frac{\lambda}{2sin\theta} \sqrt{h^2 + k^2 + l^2}$$

a :is the lattice parameter,

θ : The diffraction peak position,

(h, k, l): are called the Miller indices corresponding to the diffracting planes.

Crystallites size

Crystalline materials are aggregates of a multitude of sometimes very small crystals. In these poly-crystals, the ordered character of matter is present at the scale of each crystal. Metals and metal alloys fall within this description. Crystals in the aggregates are called grains and the boundaries between them are called grains boundaries. The grain boundaries area is made up of atoms that have no crystal structure (disordered area).

- **Micro deformations**

A crystal has defects (network defects) even if they are few in number. These defects are of considerable importance since they determine many important properties of crystalline solids, such as plastic properties. There are four kinds of crystalline defects:

- Point defects: causes a defect around a point.
- Linear defects: linear faults called dislocations (wedge dislocations and screw dislocations).
- Plane defects: two-dimensional defects including grain boundaries, twins, sub-joints and anti-phase walls.
- Three-dimensional defects: we have a three-dimensional defect when a volume of a different compound replaces a part of the crystal.

I.6.1.3 Halder- Wagner method

Microstructural evaluation is important to understand physical and chemical properties of polycrystalline materials, particularly in the field of nanotechnology. The latest version of a multi-purpose pattern-fitting system offers new features of Williamson–Hall (WH) and Halder–Wagner (HW) methods to determine crystallite sizes and micro- deformations from integral breadths β of powderdiffraction data.
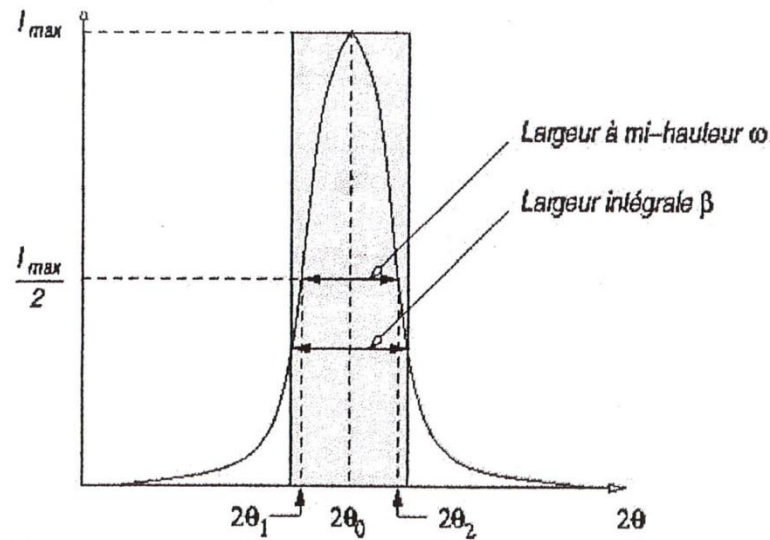
Figure I.7: X-Ray diffraction parameters.

Halder-Wagner's theory links the grain size and the accumulated micro-deformations in the crystalline structure by a right equation of the shape y=ax+b for which the slope gives the grain size and the y-axis gives the percentage of the micro-deformations:

$$\left(\frac{\beta_{sample}}{d*}\right)^2 = \frac{1}{d}\left(\frac{\beta_{sample}}{d*^2}\right) + \frac{\varepsilon^2}{4} \quad (2)$$

β_sample is the reduced (normalized) integral breadth (divided by λ) of a diffraction peak corresponding to a powder sample:

$$\beta_{sample} = \beta_{\exp} - \frac{\beta_{inst}^2}{\beta_{\exp}} \quad (3)$$

$$\beta_{sample} = \beta\frac{\cos\theta}{\lambda}(4)$$

$$\beta_{sample} = \frac{\int I(2\theta)d(2\theta)}{I_{max}}(5)$$

d*is called the reticular distance of the reduced reciprocal system (distance between two crystallographic planes):

$$d* = \frac{2\sin 2\theta}{\lambda} \ (6)$$

2θis the angle of Bragg (diffraction), and λ is the wavelength of X-ray radiation.

I.6.2 Electronic Microscopy

I.6.2.1 Transmission Electron Microscopy

Transmission electron microscopy (TEM) is applied to reveal sub-micrometer, internal fine structure in solids. Materials scientists tend to call this microstructure while bioscientists usually prefer the term ultrastructure. The amount and scale of the information, which can be extracted by TEM, depends critically on four parameters [17]:

- the resolving power of the microscope (usually smaller than 0.3 nm),
- the energy spread of the electron beam (often several eV),
- the thickness of the specimen (almost always significantly less than 1 μm),
- the composition and stability of the specimen.

The first and second of these depend largely on the depth of pocket – the more you spend, the better the microscope parameters. The third is usually determined by the experimental skill while the last depends on luck or choice of experimental system.

The two available types of transmission electron microscopy CTEM and STEM – differ principally in the way they address the specimen. The conventional TEM (CTEM) is a wide-beam technique, in which a close-to-parallel electron beam floods the whole area of interest and the image, formed by an imaging (objective) lens after the thin specimen from perhaps 106 pixels, is collected in parallel. The scanning TEM (STEM) deploys a fine focused beam, formed by a probe-forming lens before the thin specimen, to address each pixel in series as the probe is scanned across the specimen. In both types of instrument, analytical information from a small region is usually collected using a focused beam. The smallest region from which an analysis can be collected is defined by the diameter of this beam and hence the corresponding through-thickness volume in the specimen within which various inelastic scattering (energy-loss) processes take place.

I.6.2.2 Scanning Electron Microscopy

Scanning electron microscopy (SEM)is a versatile advanced instrument, which is largely employed to observe the surface phenomena of the materials. The sample is shot in a scanning electron microscope using high-energy electron, and the out coming electronsare analyzed. These out coming electrons give information about topography, morphology, composition, orientation of grains, crystallographic information, etc. of a material. Morphology indicates the shape and size, while topography indicates the surface features of an object or "how it looks", its texture, smoothness or roughness. Likewise, composition means elements and compounds that constitute the material, while crystallography means the arrangement of atoms in the materials. SEM is the leading apparatus that is capable of achieving a detailed visual image of a particle with high qualityand spatial resolution of 1 nm. Magnifications of this kind of apparatus can extend up to 300,000 times [18].

Although SEM is used just to visualize surface images of a material (does not give any internal information), it is still considered as a powerful instrument that can be used in characterizing crystallographic, magnetic and electrical features of the sample and in determining if any morphological changes of the particle has occurred after modifying the sample surface with other molecules.

There are certain differences between a scanning electron microscope (SEM) and a transmission electron microscope (TEM) thatare given as below:

- SEM detects scattered electrons emitted from the surface of the sample, while TEM detects transmitted electrons,

- SEM provides information about surface morphology and composition of materials while TEM gives details about internal composition of materials. Thus, TEM can illustrate several characters of a material (morphology, crystallization, stress or even magnetic domains),

- Both need electrically conductive materials to be tested. Non-conductive materials should be coated with a conductive layer of metal or carbon,

- The accelerated voltage ranges from 10 to 40 kV for the SEM, while for TEM, it is >100 kV,

- SEM requires a very easy preparation technique, while TEM needs skill to prepare a very thin sample. The thickness of the specimen is not important in SEM, while specimen thickness is very important in TEM. The thickness of the specimens to be examined under TEM should be less than 100 nm. SEM is a better tool for surface characterization as compared to TEM, which is better for internal structure analysis,

- The resolution is much higher in TEM as compared to SEM,

- TEM is used for high magnification compared to SEM,

- In the case of SEM, the electron beam scans over the surface of the sample, while in the case of TEM, the electron beam passes through the sample,

- SEM has a comparatively low resolution than TEM, while TEM has high resolution,

- SEM has a high depth of field, while TEM has moderate,

- SEM has lower magnifying power, while TEM has high magnifying power,

- In SEM, the specimen contrast is by electron absorption, while it is by electron scattering in TEM,

- SEM produces three-dimensional black and white images, while TEM produces two-dimensional black and white images.

Conclusion

This first chapter is dedicated to a bibliographic study of the aircraft coatings and their evolution with the advent of nanomaterials. A special interest is focused on the nanocomposite coatings for aircrafts. Preparative methods and nanomaterials elaboration are as well as the characterization tools and analysis methods are presented.

Chapter II: Microwave and material mediums

Introduction

In microwaves Material's medium are characterized by their dielectric permittivity and magnetic permeability behavior according to frequency. These electromagnetic properties are of fundamental importance in physics and engineering, since they determine the response of the material to electromagnetic fields. Usually, such properties are extracted from the scattering Parameters (S matrix) of circuits and devices at RF, VHF, UHF, microwave and mm-wave frequencies, which can be measured by a Vector Network Analyzer (VNA).

II.1   Microwave band

Microwaves represent a frequency band between 300MHz and 300GHz, which therefore characterizes signals with a wavelength between 1m and 1 mm. These limits make possible to locate the microwave domain between that of the waves used for radio broadcasting (lower frequency) and that of infrared rays (higher frequency).
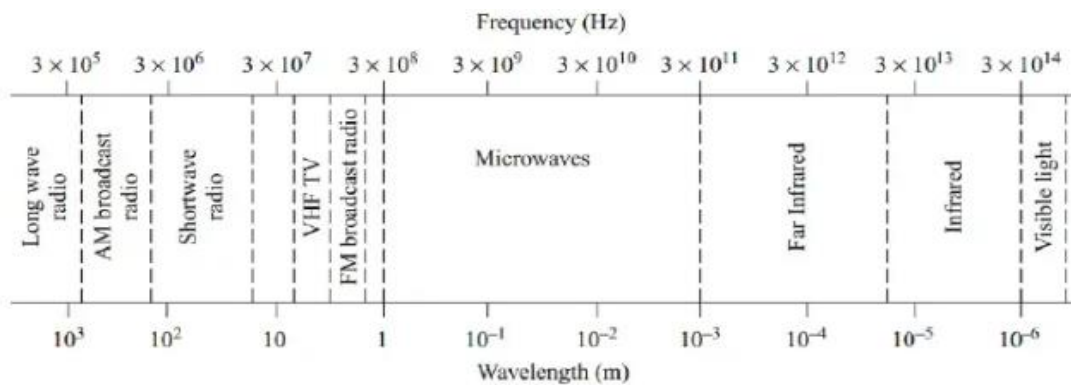

Figure II.1 microwave frequencies and the corresponding wavelengths

Microwaves properties can be listed as follows:

- Short wavelengths,
- Larger bandwidth
- At higher frequencies, more antennagain can be obtained for a given physical antenna size.
- Reflection from metallic surfaces.
- Transparency to the ionosphere,

- Low electromagnetic noise from 1 to 10 GHz,
- Microwave heating.

Consequently, several applications are defined in the microwaves range to benefit the Aeronautic sector.

An electromagnetic radiation is a self-propagating wave in space or through matter, and it has both electrical and magnetic components that oscillate in phase normallyto each other and in the direction of the propagation of the wave or energy.It is defined by its propagation speed (300 000 km/s in a vacuum), amplitude, and wavelength or frequency.

II.2 Dielectric Permittivity

In microwaves, dielectric permittivity (typically denoted by the symbol ε) is one of the fundamental material parameters; it is a diagnostic physical property, which characterizes the degree of electrical polarization of a material experiences under the influence of an external electric field[19].

Dielectric materials exist in solid, liquid and gaseous form. They are able to store electrical energy, since they allow the electric field to penetrate them; this penetration ability is characterized by their electrical permittivity.Ideal dielectric materials are materials that do not conduct electrical current since they do not contain free charges in their structures, unless they are subjected to the action of external ionizing factors causing the loss of their dielectric properties. Also, the charges of different signs in the atoms and the particles of the dielectrics are linked. When these charges are subjected to the forces induced by the electric field, some of these connections do not break but only slight elastic displacements appear.All the positive charges move in the direction conforming to that of the field, and the negative charges in the opposite direction, which creates a polarization of the dielectric. Any mobility of charge carriers, induce dielectric losses. All phenomena in dielectrics subjected to an electric field depend on the frequency of the field, the temperature and the structure of the dielectric.

II.2.1 polarization phenomenon

The dielectric losses are due to the movements of the charge carriers. The effect ofthe movements of the charge carriersis called induced polarization. Michael Faraday had discovered the effect of dielectric polarization in 1837.

The polarization phenomenon can be explained by two charged plates separated with equal and opposite charges on either side. When there is no material (vacuum) between the two plates there will exist an Electric Field directed downward (from the positive charge to the negative charge).When there is a material placed between the plates. This material is no doubt made up of atoms which often form molecules. These molecules will often have some sort of dipole moment. In the absence of an external electric field, these molecules will align randomly.When the plates are charged the result is that the molecules are aligned by their dipole moment and the external electric field. The electric field due to the dipole moment of the materials molecules opposes the external electric field E The result is that the net electric field is reduced within the material.The permittivity is a measure of how much the molecules oppose the external E-field.
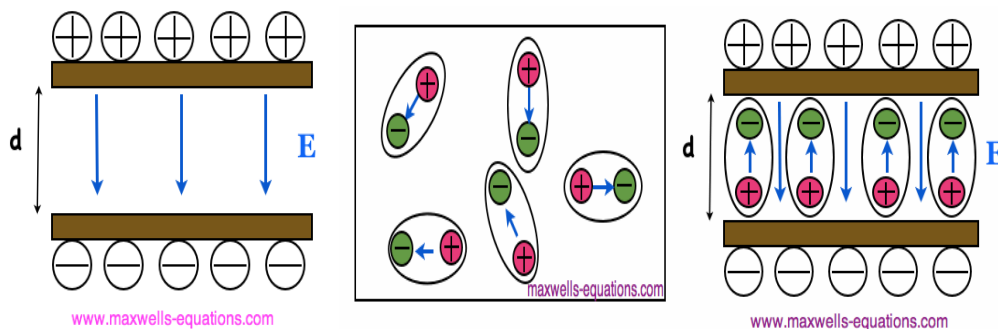
Figure II.2: the polarization phenomena

II.2.2 polarization types

There are several types of polarization, which can co-exist or appear separately. All these types of polarization can be classified into two groups according to their characteristics:

- Elastic polarization (or resonance)
- Relaxation polarization.

Total polarization is the sum of the different types of polarization.

- **Electronic polarization:** elastic displacement and electron orbits deformation in atoms and ions. Electronic polarization is inherent to all the dielectrics (instantaneous phenomenon: 10^{-15}s) and disappears with the suppression of the applied field.
- **Ionic (or atomic) polarization:** results from the displacement of bound atoms by ionic bonds. In this case, valence electrons travel through shared orbits with other

atoms. The ionic polarization creates induced dipoles; it does not cause energy loss and disappears with the suppression of the applied field.

➢ Electronic and ionic polarizations are elastic polarization character. It disappears with the suppression of the applied field.
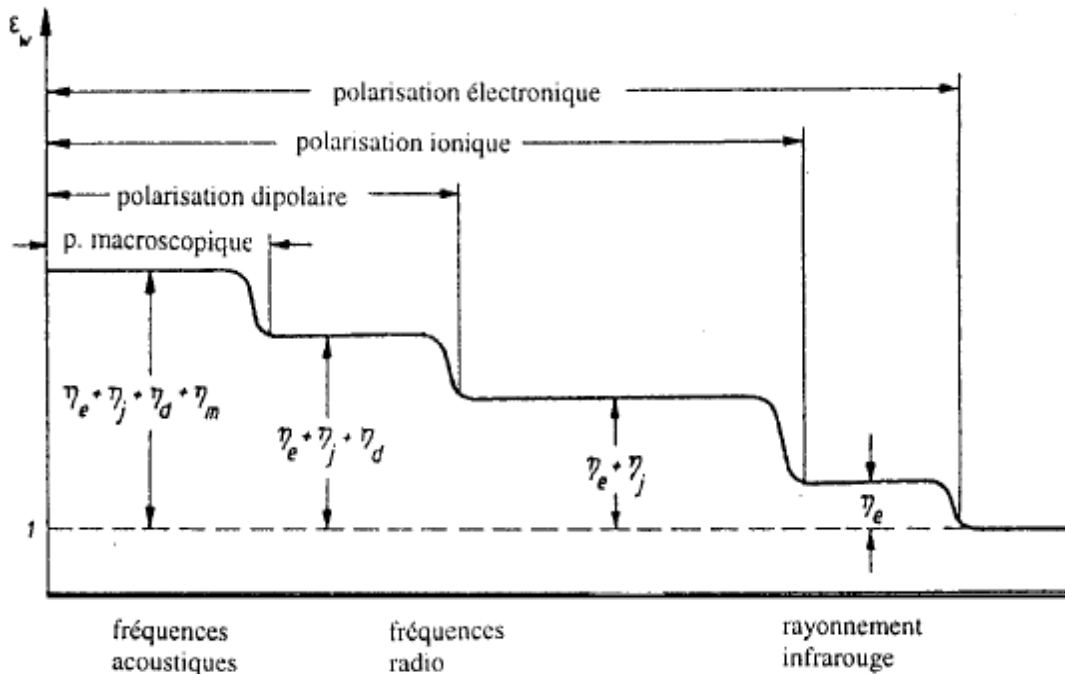
Figure II.3 dielectric permittivity variation to different frequencies

- **Dipolar (orientation) polarization:**

Characterized by partial an orientation of polar molecules under the action of an electric field such molecules are asymmetric structure where the gravity center of all the negative charges does not coincide with the gravity center of all the positive charges.

- **Macroscopic polarization (spatial load polarization)**:

Describes the process of limited displacement of free loads. It can be encountered in liquid and solid dielectrics, especially with a non-homogeneous or amorphous structure.

- **Interfacial (Maxwell- Wagner type) polarization:**

Appears in the non-homogenous dielectrics. It occurs when there is an accumulation of charges at an interface between two materials or between two regions within a material because of an external field.

- **Spontaneous polarization:**

Occurs in materials characterized by the presence of regions called domains comprising identically polarized particles. The domains, disordered at first, orient themselves when an external field is applied.

Dipolar, macroscopic and interfacial polarizations are relaxation polarization character. This lastgathers all the mechanisms in which, under the action of the field, a displacement of connected loads takes places,leadingto a disorganizationof the medium structure.The change in orientationdoes not occur immediately, but with a delay (relaxation) compared to the changes in the external electric field.
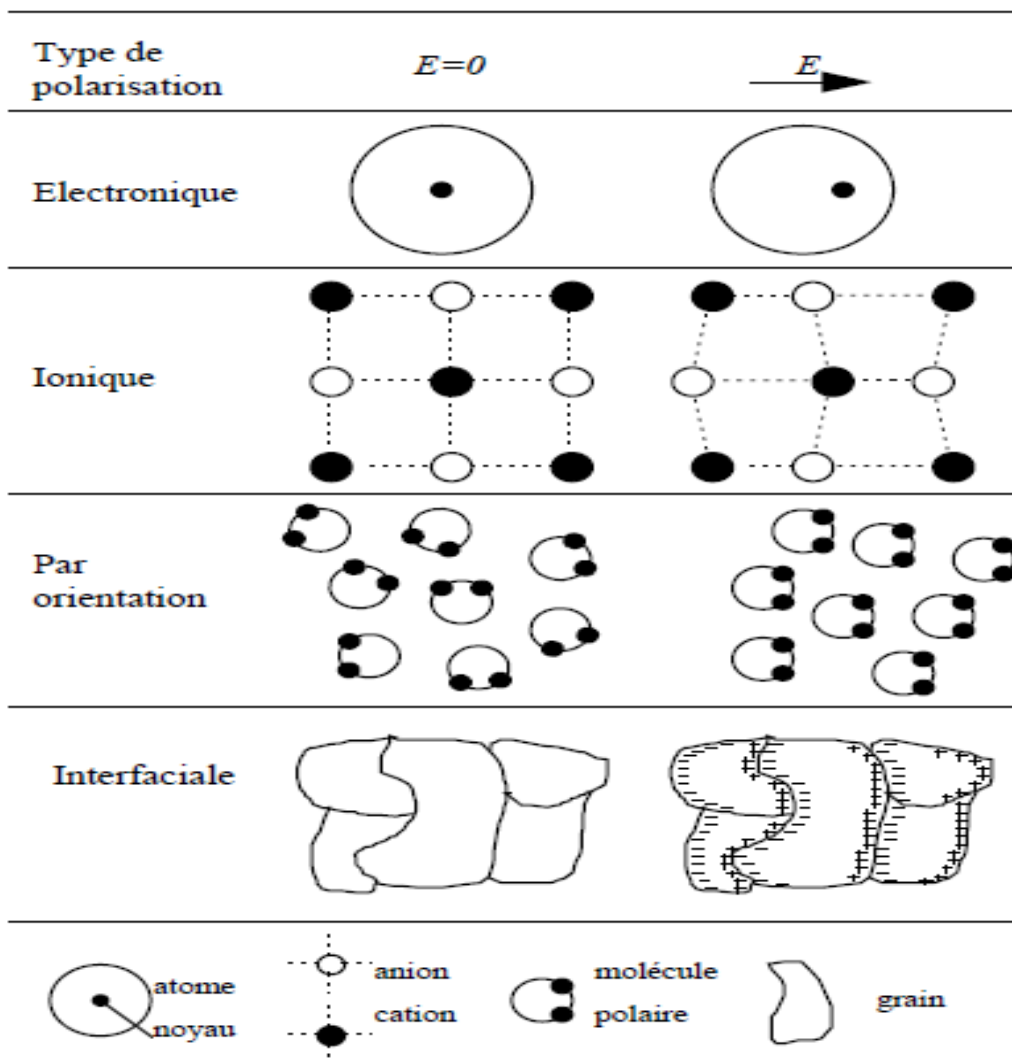
Table II.1 the different types of polarization

II.2.3 Complex permittivity and dielectric losses

A dielectric is characterized by its relative permittivity or dielectric constant εr. In the case of a perfect dielectric, ε_r is the quotient of the capacitance Cx between two electrodes, assumed to be embedded in this dielectric, by the capacitance Cv of the same configuration of electrodes in a vacuum:

$$\varepsilon_r = \frac{Cx}{Cv} \qquad \text{(II.1)}$$

✓ Absolute permittivity ε is the product of relative permittivity εr by vacuum permittivity ε0 (ε0 = 8,85. 10-12 F/m):

$$\varepsilon = \varepsilon_r \varepsilon_0 \qquad \text{(II.2)}$$

Absolute permittivity defines the possibility of being crossed by an electric current, under the action of the electric field. Indeed, the current density *J(t)* passing through this dielectric in the presence of a sinusoidal electric field *E(t)* is:

$$J(t) = \sigma E(t) + \frac{\partial D(t)}{\partial t} \qquad \text{(II.3)}$$

- D is the electric flux density and σ is the conductivity.

Through the Fourier Transformation, we will have:

$$J(\omega) = \sigma E(\omega) + j\omega D(\omega) \qquad \text{(II.4)}$$

$$J(\omega) = [\sigma + j\omega\varepsilon_0(1 + x'(\omega) - jx''(\omega))]E(\omega) \text{(II.5)}$$

$$J(\omega) = [\sigma_c + \omega\varepsilon''(\omega) + j\omega\varepsilon'(\omega)]E(\omega) \qquad \text{(II.6)}$$

Where:

$$\varepsilon_0(1 + x'(\omega) - jx''(\omega)) = \varepsilon'(\omega) + j\varepsilon''(\omega) = \varepsilon^*(\omega) \qquad \text{(II.7)}$$

x' and *x''* are the real and imaginary components of the electrical susceptibility *x* of the medium. ε 'and ε'' are the real and imaginary components of the complex electrical permittivity ε of the medium. The complex permittivity takes into account the energy dissipation, absorption and diffusion losses. We also define a relative complex permittivity:

$$\varepsilon_r{}^* = \varepsilon_r{}' - \varepsilon_r{}'' \qquad\qquad (II.8)$$

Where$\varepsilon_r{}'$ plays the role that ε_r had in the case of perfect insulators. The absolute complex permittivity is, in the same way, equal to the product of the relative complex permittivity by ε_0.

The phase component presented by J with E is responsible for dielectric losses; it represents the dissipation of the power in the dielectric. These losses are due to the necessary work for establishing the polarization and residual conduction σ_c of the dielectric. The dielectric dissipation factor is equal to the quotient$\dfrac{\varepsilon''_r}{\varepsilon'_r}$; this quotient is also called the tangent of the loss angle or tanδ; δ is the complementary angle of the phase shift between the voltage applied to the dielectric and the resulting current (tan$\delta = \dfrac{\varepsilon''_r}{\varepsilon'_r}$).

II.3 Magnetic permeability

Magnetic permeability is defined as the ratio of the magnetic induction to the magnetic intensity. It is a scalar quantity and denoted by the symbol μ. Magnetic permeability helps us measure a material's resistance to the magnetic field or measure of the degree to which magnetic field can penetrate through a material. If the material has greater magnetic permeability, greater will be the conductivity for magnetic lines of force.Permeability depends on several factors such as the nature of the material, humidity, position in the medium, temperature, and frequency of the applied force.

The phenomenon behind the permeability is the magnetization. It can be explained when exposing a material to an applied magnetic field; the collection of individual magnetic dipole moments within most materials will attempt to reorient themselves along the direction of the field. This generates an induced magnetization, which contributes towards the net magnetic flux density inside the material. The degree in which the induced magnetization affects the magnetic flux density depends on the material's magnetic permeability:

$$\mu = B/H \quad (II.1)$$

With B is the magnetic intensity and is H the magnetizing field.

A useful tool for dealing with high frequency magnetic effect is the complex permeability. While at low frequencies in linear material, the magnetic field and the auxiliary magnetic field

are simply proportional to each other through some scalar permeability. At high frequencies, these quantities will react to each other with some lag time. These fields can be written as phases such that:

$$H=H_0 e^{jwt} \quad (II.2)$$

And,

$$B=B_0 e^{j(wt-\delta)} \quad (II.3)$$

Where δ is the phase delay of B from H.

Understanding permeability as a ratio of the magnetic flux density to the magnetic field the ratio of the phases can be written as:

$$\mu=\frac{B}{H}=\frac{B_0 e j(wt-\delta)}{H_0 e jwt}=\frac{B_0}{H_0} e^{-j\delta} \quad (II.4)$$

Therefore, the permeability becomes complex number. By Euler's formula, the complex permeability can be translated from polar to rectangular form:

$$\mu=\frac{B_0}{H_0}cos\ (\delta)-j\frac{B_0}{H_0}sin\ (\delta) \quad (II.5)$$

$$\mu=\mu'-j\mu'' \quad (II.6)$$

II.4 Electromagnetic characterization methods

By electromagnetic characterization of materials, we allude to the investigation of the complex dielectric permittivity and magnetic permeability behavior over a frequency range. It is fundamental to have access to methodologies that can accurately characterize these properties of materials. Each method is limited to specific frequencies, materials and applications. Available techniques can be substantially divided into two categories[20]:

- Resonant methods: used to get accurate knowledge of dielectric properties at single frequency or several discrete frequencies.

- Non-resonant methods: often used to get a general knowledge of electromagnetic properties over a frequency range.

II.4.1 Resonant Methods

Resonant measurements are the most accurate methods of obtaining permittivity. However, there are limitations on the frequencies and loss characteristics of the materials that can be measured with the method. The dielectric properties can be determined by first measuring the resonant frequency and quality factor of an empty cavity. The second step is to repeat the measurement after filling the cavity with the MUT.The material's permittivity cans then becomputed using the frequency, volume and q-factor.
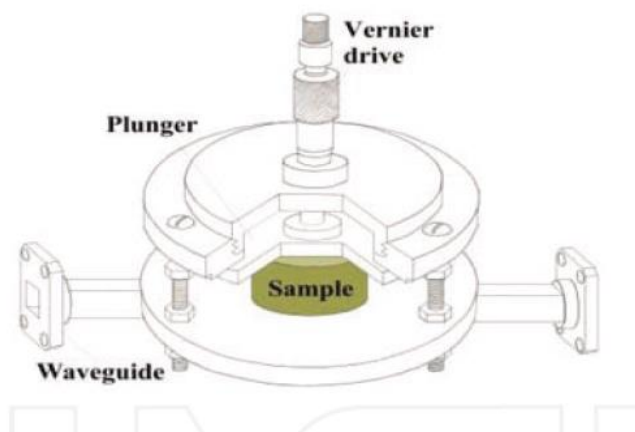
Figure II.4 Measurement of the sample using cavity resonator

Resonant methods are better accuracy and sensitivity, ability to measure very small MUT and more suitable for low-loss samples. These measurements need a high frequency resolution VNA and characterizematerials at a discrete number of frequencies.

II.4.2 Free space Methods

Free space measurement method is developed for determining the electromagnetic properties of a material under high temperatures or hostile environments and generally operates in wide band frequencies(X band). This measurement requires that the material under test (MUT) be large and flat. It consists in two antennas placed facing each other where they are connected to a vector network analyzer (VNA).Once calibrated, the MUT is then placed on the sample holder between the antennas and the s-parameter measurement is performed again.

Figure II.5Measurement of sample using free space method.
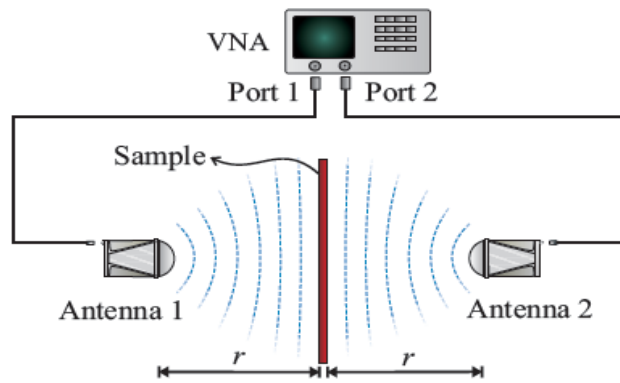
Free space measurement is wideband method; both the magnetic and dielectric properties can be evaluated and does not require contact between the sample and the antennas). However, it requires large and flat MUT and provides a less precise measurement because of multiple reflections between antenna and surface of sample and diffraction effects at the edge of sample.

II.4.3 Reflection/Transmission Methods

Microwave measurements using Transmission/Reflection line method involves placing a sample in a section of waveguide or coaxial line and measuring the two ports complex scattering parameters with a vector network analyzer (VNA). The method involves measurement of the reflected (S11) and transmitted signal (S21). The relevant scattering parameters relate closely to the complex permittivity and permeability of the material by equations. In many cases, the method requires sample preparation such as machining so that the sample fit tightly into the waveguide or the coaxial line. Waveguide methods are usually more popular since circular or rectangular samples are easier to produce than coaxial ones.
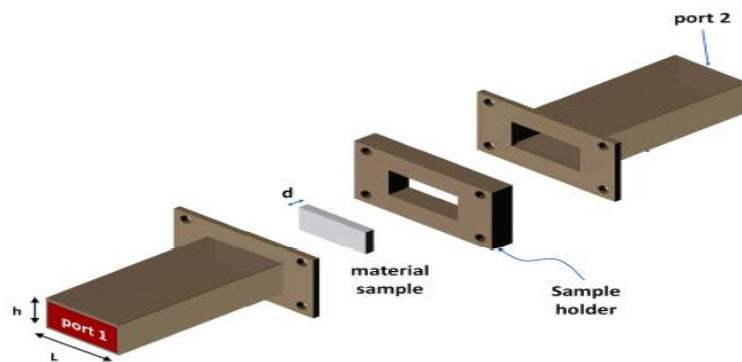

Figure II.6 Reflection/Transmission device with the material sample to be characterized: waveguide

Coaxial lines and waveguides are commonly used to measure samples with medium to high loss.It can be used to determine both the permittivity and permeability of the material under test. However the air-gap effects limit the measurement accuracy.

II.4.4 Choice Criteria

The choice of the EM characterization method depends on the EM parameters such as the frequency band and the required accuracy of the results and, more remarkably, also on the physical and mechanical parameters of the investigated specimen such as its physical state (solid, liquid), its size and shape. In this work, a X-band rectangular waveguide was on hand for electromagnetic measurements over the frequency range of 8.2 to 12.4 GHz[21].

II.5 Waveguides

The metallic rectangular guide is one of the first types of transmission lines used due to their ability to transport both great powers and high frequency signals. It consists in a hollow metallic tube filled with a material medium (ε_r, μ_r) able to propagate electromagnetic waves by reflection on the metallic walls[22].
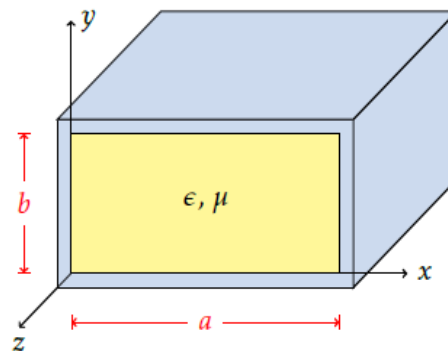
Figure II.7 Representation of the rectangular guide

The study of the wave propagation in the waveguide permits to define:

- **TE propagation mode**

The rectangular guide is a guide that has a single conductor, and therefore it cannot support TEM mode. TE and TM modes having cut-off frequencies, this type of guide has a minimum operating frequency.For TE mode, the propagation constant is:

$$\beta = \sqrt{k^2 - k_c^2} = \sqrt{k^2 - \left(\frac{m\pi}{a}\right)^2 - \left(\frac{n\pi}{b}\right)^2}$$

(II.1)

With, k is the wave number of the filled waveguide and k_c is the cut-off wave number. m and n are the half wave length on the a and b sides respectively.

Consequently, a cutoff frequency own to the waveguide is defined as follows:

$$f_{c_{mn}} = \frac{k_c}{2\pi\sqrt{\mu\epsilon}} = \frac{1}{2\pi\sqrt{\mu\epsilon}}\sqrt{\left(\frac{m\pi}{a}\right)^2 + \left(\frac{n\pi}{b}\right)^2}$$

(II.2)

The mode with the lowest cutoff frequency is called dominant mode. Since a> b, the dominant mode is TE$_{10}$ (m = 1, n = 0):

$$f_{c_{10}} = \frac{1}{2a\sqrt{\mu\epsilon}}$$

(II.3)

At an operating frequency f, only the modes having $f_c < f$ will propagate; the other modes will be strongly attenuated (evanescent modes).

- **TM propagation mode**

The TM mode has the same propagation constant and cut-off frequency as the TE mode. However, the modes TM$_{00}$, TM$_{10}$ and TM$_{01}$ do not exist. The lowest mode that propagates is TM11.

Paramètre	Mode TE$_{mn}$	Mode TM$_{mn}$
k	$\omega\sqrt{\mu\epsilon}$	$\omega\sqrt{\mu\epsilon}$
k_c	$\sqrt{(m\pi/a)^2 + (n\pi/b)^2}$	$\sqrt{(m\pi/a)^2 + (n\pi/b)^2}$
β	$\sqrt{k^2 - k_c^2}$	$\sqrt{k^2 - k_c^2}$
λ_c	$2\pi/k_c$	$2\pi/k_c$
λ_g	$2\pi/\beta$	$2\pi/\beta$
α_d	$(k^2\tan\delta)/2\beta$	$(k^2\tan\delta)/2\beta$

Table II.2 rectangularguide'sequations

II.6 Dispersion matrix S

Scattering parameters, which are commonly referred to as S-parameters, are a parameter set that relates tothe traveling waves that are scattered or reflected when an n-port network is inserted into a transmission line.

The ease with which scattering parameters can be measured makes them especially well-suited for describing microwaves circuits. Measuring most other parameters calls for the input and output of the device to be successively opened and short circuited. This can be hard to do, especially at RF frequencies where lead inductance and capacitance make short and open circuits difficult to obtain. Animportant advantage of S-parameters stems from the fact that traveling waves, unlike terminal voltages and currents, do not vary in magnitude at points along a lossless transmission line. This means that scattering parameters can be measured on a device located at some distance from the measurement transducers, provided that the measuring device and the transducers are connected by low-loss transmission lines[23].
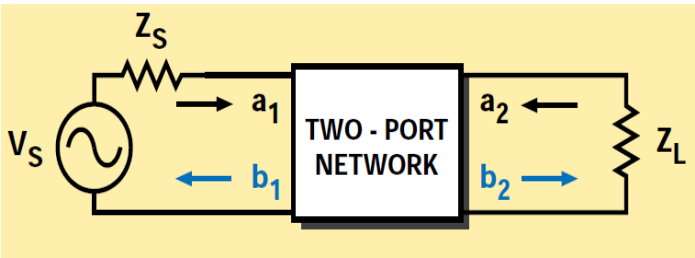

Figure II.8 The S parameters give information about the behavior of a circuit

From there we get the s-parameters s11, s22, s21, and s12:

$$s_{11} = \left. \frac{b_1}{a_1} \right|_{a_2=0} = \text{Input reflection coefficient with the output port terminated by a matched load } (Z_L = Z_0 \text{ sets } a_2 = 0)$$

$$s_{22} = \left. \frac{b_2}{a_2} \right|_{a_1=0} = \text{Output reflection coefficient with the input terminated by a matched load } (Z_S = Z_0 \text{ sets } V_s = 0)$$

$$s_{21} = \left. \frac{b_2}{a_1} \right|_{a_2=0} = \text{Forward transmission (insertion) gain with the output port terminated in a matched load.}$$

$$s_{12} = \left. \frac{b_1}{a_2} \right|_{a_1=0} = \text{Reverse transmission (insertion) gain with the input port terminated in a matched load.}$$

Scattering parameters turn out to be particularly convenient in many network calculations. This is especially true for power and power gain calculations. The transfer parameters s12 and s21 are a measure of the complex insertion gain, and the driving point parameters s11 and s22 are a measure of the input and output mismatch loss. As dimensionless expressions of gain and reflection, the s-parameters not only give a clear and meaningful physical interpretation of the network performance, but also form a natural set of

parameters for use with signal flow graphs. It is not necessary to use signal flow graphs in order to use s-parameters, but flow graphs make s-parameter calculations extremely simple.In a signal flow graph, each port is represented by two nodes. Node an represents the wave coming into the device from another device at port n, and node bn represents the wave leaving the device at port n. The complex scattering coefficients are then represented as multipliers on branches connecting the nodes within the network and in adjacent networks[24].
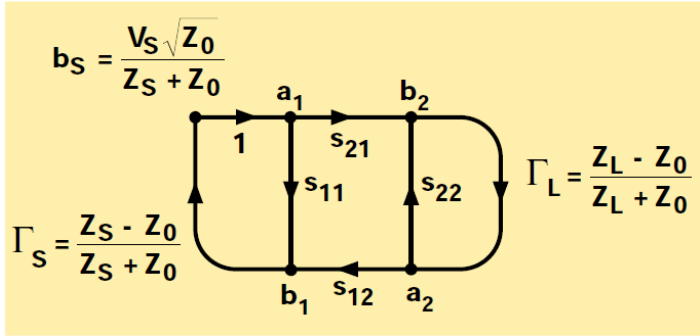

Figure II.9 the simplification of network analysis by flow graphsresults

The simplification of network analysis by flow graphsresults from the application of the non-touching loop rule. This rule applies a generalized formula to determine the transfer function between any two nodes within a complex system.

II.7 NRW Extraction Method

By extraction method, we mean a conversion process of the measured S parameters into relative dielectric and magnetic permeability magnitude. Basically, the complex permittivity and permeability of material's mediums are extracted by reflection (S21) and/or transmission (S11) parameters, which are called as scattering parameters. In these processes, many techniques such as Nicholson-Ross-Weir (NRW), NIST, Root Find Algorithm (RFA), and Genetic Algorithm (GA) are used .The techniques used in the extraction process can be divided into two main categories as analytical and numerical.The results, obtained from analyzed data by the extraction techniques, give an approximate value to the results of the mathematical theory. By optimizing these analytical and numerical techniques, the complex permittivity and refractive index of materials can be extracted with a smaller error rate and higher accuracy. To obtain accurate results, the extraction techniques should be compared according to the above criteria and the most suitable one should be determined[20].

One of the most popular methods for material's electromagnetic parameters extraction is the Nicolson–Ross–Weir (NRW) algorithm, based on T/R measurements of the specimen under test. The propertiesof materials are retrieved from their impedance and the wave velocities in the materials. It is well known that the main drawback of this method is related to the electrical thickness of the analyzed material. NRW algorithm processes the advantages of fast, non-iterative and applicable to waveguides and coaxial line. However the method in not suitable for low loss materials and shows divergence at frequencies corresponding to multiples of one-half wavelengths.

In the NRW algorithm, the presences of a sample of thickness d in the transmission line induce a phase factor T defined as:

$$T = e^{-j\,k\,d} = e^{-\gamma\,d}.$$

$$(II.1)$$

The reflection coefficient at the first interface between the empty transmission line's section and the filled one is:

$$\Gamma = \frac{Z_1 - Z_0}{Z_1 + Z_0} \qquad\qquad (II.2)$$

Where Z_0 and Z_1 are the transmission line's characteristic impedances in absence and in the presence of the sample respectively.

According to the theory of multiple reflections, the scattering parameters of the finite length sample (S11 and S21) can be written as a function of the reflection coefficient at the interface of two infinite media Γ and as a function of the phase factor T:

$$S_{11} = \Gamma_{IN} = \frac{\Gamma(1 - T^2)}{1 - \Gamma^2 T^2}, \; S_{21} = \frac{(1 - \Gamma^2)T}{1 - \Gamma^2 T^2}.$$

$$(II.3)$$

At this point, the reflection coefficient Γ, which contains the impedance of the unknown medium, and the phase factor T, which contains the propagation constant of the unknown medium, can be expressed as a function of the scattering parameters of the sample :

$$\begin{cases} \Gamma = K \pm \sqrt{K^2 - 1} \\ T = \frac{S_{11} + S_{21} - \Gamma}{1 - (S_{11} + S_{21})\Gamma} \end{cases}.$$

$$(\text{II}.4)$$

Where the auxiliary parameter K is a function of the scattering parameters S11 and S21:

$$K = \frac{S_{11}^2 - S_{21}^2 + 1}{2S_{11}}.$$

$$(\text{II}.5)$$

The phase factor T of relation (II.1)is complex:

$$T = e^{-\gamma d} = |T| e^{-j\phi}.$$

$$(\text{II}.6)$$

Consequently, the propagation constant γ can be obtained by applying the natural logarithm of the complex variable T:

$$\gamma = jk = \frac{1}{d}[-\ln(|T|) - j\phi + j2\pi n], \ n = \ldots -2, -1, 0, 1, 2 \ldots$$

$$(\text{II}.7)$$

Once γ is calculated, it is possible to estimate the electrical permittivity and the magnetic permeability:

$$\Gamma = \frac{Z_1 - Z_0}{Z_1 + Z_0} = \frac{Z_0\sqrt{\frac{\mu_r}{\varepsilon_r}} - Z_0}{Z_0\sqrt{\frac{\mu_r}{\varepsilon_r}} + Z_0} \qquad (\text{II}.8)$$

This leads to:

$$\frac{1+\Gamma}{1-\Gamma} = \sqrt{\frac{\mu_r}{\varepsilon_r}} \qquad (\text{II}.9)$$

Considering that:

$$\gamma = jk = j\omega\sqrt{\mu\varepsilon} \qquad (\text{II}.10)$$

$$\frac{\gamma}{\gamma_0} = \sqrt{\mu_r \varepsilon_r}$$

So:

$$\frac{1+\Gamma}{1-\Gamma} = \frac{1}{\varepsilon_r}\frac{\gamma}{\gamma_0} \qquad (\text{II}.11)$$

And:

$$\frac{1-\Gamma}{1+\Gamma} = \frac{1}{\mu_r}\frac{\gamma}{\gamma_0} \quad (II.12)$$

Finally:

$$\begin{cases} \varepsilon_r = \dfrac{\gamma}{\gamma_0}\dfrac{1-\Gamma}{1+\Gamma} \\ \mu_r = \dfrac{\gamma}{\gamma_0}\dfrac{1+\Gamma}{1-\Gamma} \end{cases} \qquad (II.13)$$

In a metallic rectangular waveguide environment, the magnetic permeability can be similarly calculated by using the equivalent transmission line circuit of the waveguide:

$$\mu^* = \frac{\gamma}{\gamma_0}\frac{Z^{TE}}{Z_0^{TE}} = \frac{\sqrt{k_0^2\varepsilon_r\mu_r - k_t^2}}{\sqrt{k_0^2 - k_t^2}}\frac{\omega\mu_0\mu_r}{\sqrt{k_0^2\varepsilon_r\mu_r - k_t^2}}\frac{\sqrt{k_0^2 - k_t^2}}{\omega\mu_0} = \mu_r, \qquad (II.14)$$

Where k0 is the propagation constant in free space and kt is the cutoff wave number of the waveguide. On the contrary, the dielectric permittivity should be derived from the propagation constant k :

$$(k = \sqrt{k_0\varepsilon_r\mu_r - k_t^2}) \qquad (II.15)$$

After the derivation of the magnetic permeability:

$$\varepsilon_r = \frac{k^2 + k_t^2}{k_0^2\mu^*}. \qquad (II.16)$$

Conclusion:

This second chapter is dedicated to the electromagnetic characterization: a description of the electromagnetic properties both permittivity and permeability and the different methods that can be used in order to characterize these properties of materials. A description of the NRW (Nicholson Ross weir) extraction method to obtain and extract the electromagnetic properties.

Chapter III: structural characterization and results

Introduction

In our study, we considera polymer- based nanocomposite. It consists in an epoxy resin matrix reinforced with $Fe_{60}Co_{40}$ nanocrystalline powders. By nanocrystalline powders, we mean nanostructured powders with ultra-fine grains of less than 100 nm diameter. Nanocrystalline powders are often produced via the severe plastic deformation technique (mechanical procedure). Such study requires the following steps: firstly, preparation of the fillers, secondly, elaboration of the nanocomposites samples test and finally we conduct a structural characterization in order to investigate the structural properties of the elaborated powders.

III.1 Experimental

III.1.1 Elaboration of the $Fe_{40}Co_{60}$ nanocrystalline powders

Mechanical alloying as one of the severe plastic deformation methods is a solid-state reaction process. It is a simple processing route at low temperature, which leads to significant grain refinement opening the way to new properties.

Elemental powders of Fe (99.9%, 50 Em) and Co (99.9%, 10 Em) are used as startingmaterials in nominal composition $Fe_{40}Co_{60}$ (massive ratio). High-energy mechanical alloying is performed using a Retsch PM400 planetary ball mill available at Houari Boumediene University of Science and Technology and equipped with hardened steel balls (18) and vials (4). The powders are milled with a ball-to- powder mass ratio of 50:1 anda milling intensity of 360 rpm. Vial charging and all powder handling are performed underprotective atmosphere of argon.Small samples of powders are taken after selected millingtimes for structural characterization. The nanocrystalline $Fe_{40}Co_{60}$ powders, will serve as fillers for the sample test nanocomposites.
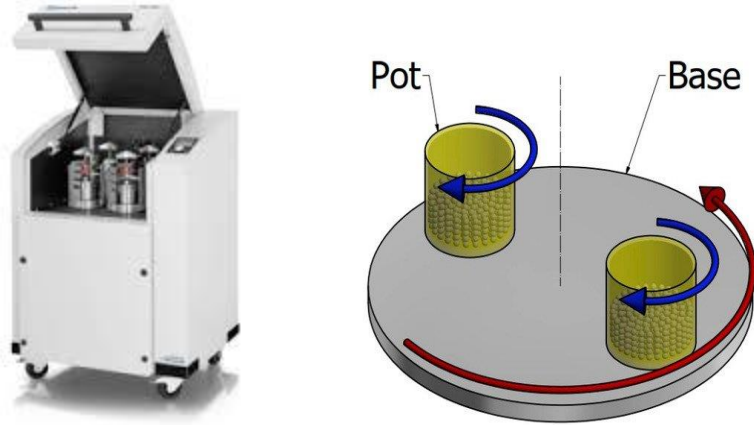
Figure III.1: Planetary ball mill.

III.1.2 Elaboration of the polymer nanocomposites

To prepare the samples test, a percentage of 30% vol. of the nanocrystalline $Fe_{40}Co_{60}$ powders is incorporated into epoxy resin matrix to form a polymer- based nanocomposite. It is a kind of organic-Inorganic 0-Dimension nanocomposite (3-Dimension in nanometer scale) prepared by the solution dispersion method. FigIII.2 shows the corresponding nanocomposites photographs.

Figure III.2: Elaborated sample tests.

III.1.3 XRD Characterization

An X- ray is an electromagnetic wave of high- frequency extending from 10^{16} to 10^{20} Hz and very short wavelength (10^{-8} to 10^{-12} m) of the order of the interatomic distances. Its energy is between 40 and 4.10^5 eV. Crossing a crystal, X- rays undergo a diffraction. Induced changes inform about the structural properties of the matter.

X-ray pattern spectra from elemental Fe and Co powders and changes with milling time for MA powders are recorded in Fig III.3 using a SIEMENS D500 diffractometer with CuKα₁ radiation of 0.1540598 nm wavelength and 0.026^o step.
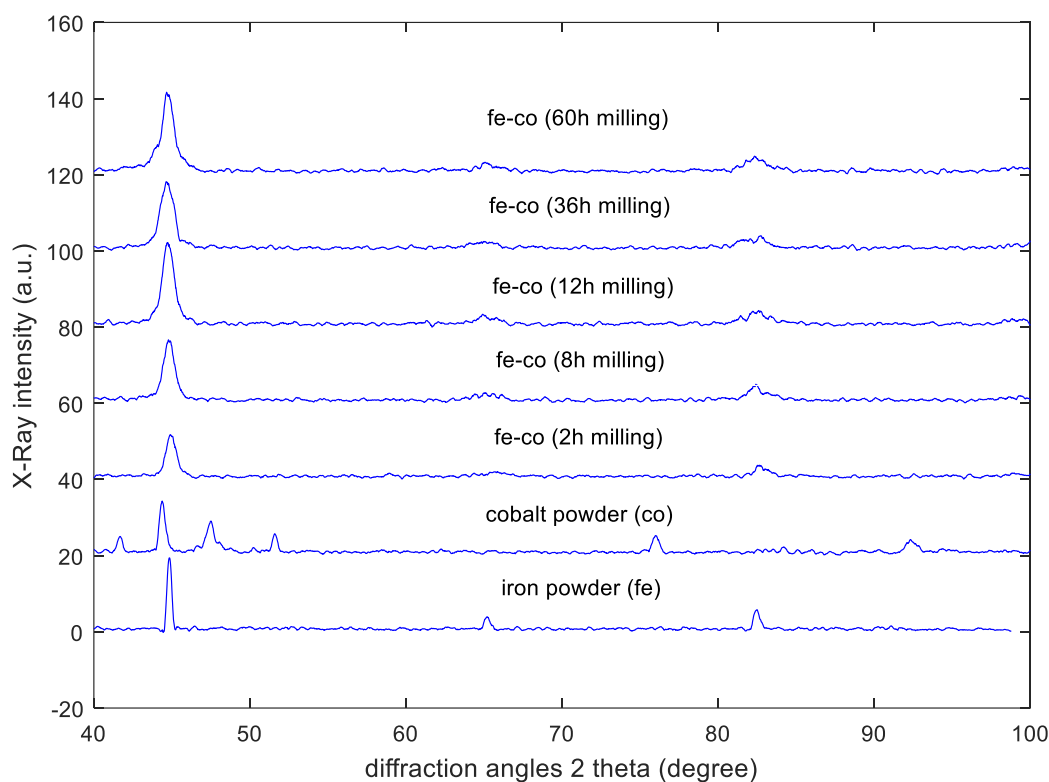

Figure III.3: Recorded XRD spectra of elemental and MA FE₄₀CO₆₀ powders.

The pure Fe spectrum in Fig III.3 indicates that the elemental Fe powder used in this elaboration is bcc structure. The main peaks of the elemental Fe powder are needle shape due to its coarse grain size.As we can see,with milling progression, the coarse Fe diffraction peaks widen and their intensity decreases. Co peaks completely disappear confirming the diffusion of the Co phase into the Fe structure. This confirms that the alloying formation occurs in a solid state during the milling process. A slight shift changes in Fe Bragg angle's accompanies this behaviourdue to continuous severe plastic deformations accumulated between balls and container's walls. The conservation of the diffraction peaks testifies about the crystalline structure obtained after powder's mechanical alloying. The peaks needle shape disappears due to the refinement grains size. Extended mechanical alloying to 60 h leads to the persistence of the peaks enlargement, decrease and disappearance of the needle shape.
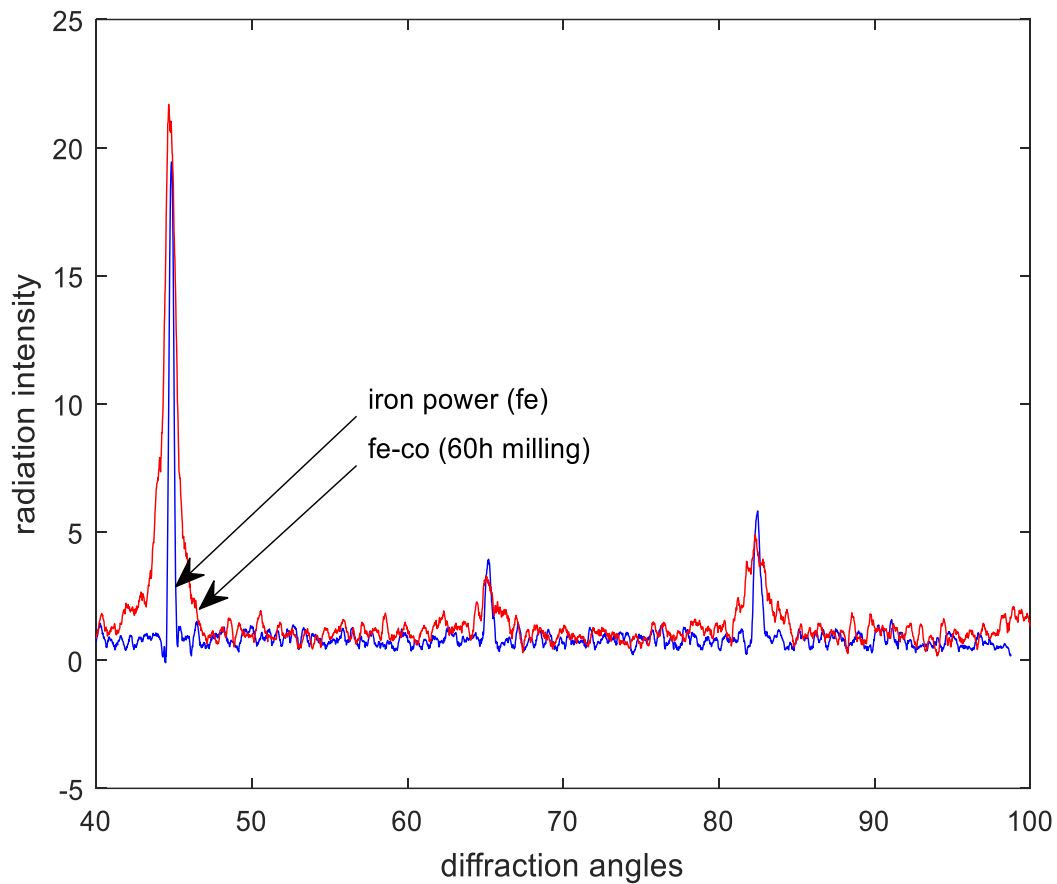
FigureIII.4: Recorded XRD spectra of elemental and MA Fe and Fe-Co after 60h of milling.

III.2 XRD analysis

To extract the desired structural parameters, we use recorded information around the main diffraction peaks given by the XRD diffractometer (Annex B).

III.2.1 Lattice parameter calculation

The lattice parameter is determined using the Bragg relation. Fig. III.5 shows the Fe lattice parameter's evolution according to milling progression for the three peaks of the XRD spectra. The variation of the lattice parameters due to the slight Bragg angles moving confirms the alloying formation by diffusion of the Co phase in the Fe matrix. The severe plastic deformations accumulated during mechanical milling contribute also to the lattice parameter variation.
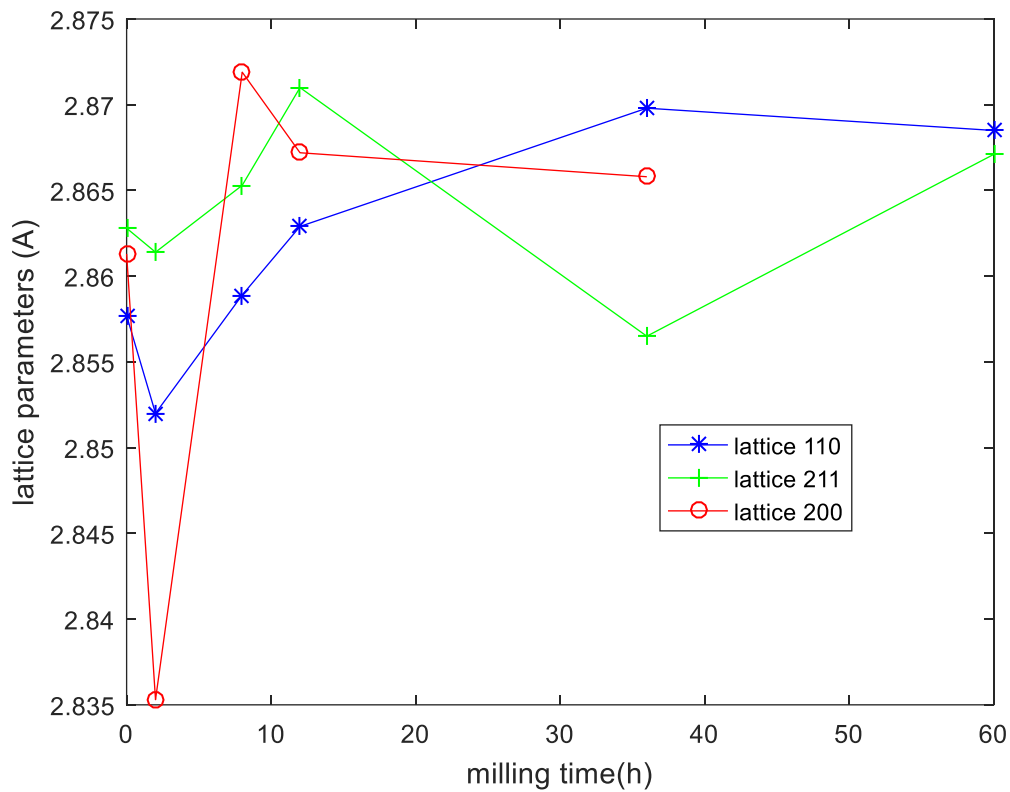
Figure III.5: Lattice parameter's evolution according to milling progression for the three peaks of the XRD spectra.

Blue(lattice 110), red(lattice 200), green(lattice 211)

III.2.2 Crystallites size and micro-deformations calculation

The Halder- Wagner method is used as analysis tool to extract mean values of the structural parameters from the recorded XRD spectra. The Halder- Wagner theory is based on the use of the integral breadth of the diffraction peaks. It links the average grain size and the residual micro- deformations in a right equation ($y = ax + b$) for which the slope gives us the average grain size and the ordered at the origin provides the residual micro- deformations.

Obtained results after calculation via the Halder- Wagner approach around the main peaks for the elemental and MA powders are:

- **for pure Co powder**

Localized diffraction angles (diffractometer data in degrees):

$$2\theta = [41.679, \quad 44.377, \quad 47.481, \quad 51.599, \quad 75.997, \quad 84.195, \quad 92.335]$$

$$X = 10^{-4}.[21,23\, , \qquad 7.4115\, , \qquad 4.2019\, , \qquad 21.321\, , 12\, , \qquad 6.2650]$$

$$Y = 10^{-5}.[9.4611\, , 14.27\, , 3.5056\, , 1.3362\, , \quad 10.916\, , 4.2463\, , 3.4395]$$

Figure III.6: Calculation of the mean crystalline size and micro deformation.

The calculated points serve to trace a right line for which:

- the slope worth's: $a = 0.0647$
- the ordered at the origin value is: $b = 0.0000061506$

Which allow to:

- a calculated mean grain size of: $d = 15.4517$ nm
- a calculated micro- deformations percentage of: $\varepsilon = 0.5\%$

- **for pure Fe powder**

Localized diffraction angles (diffractometer data in degrees):

$$2\theta = [44.838,\ 65.186,\ 82.5]$$

$$X = [0.0015, \qquad 0.00090672, \qquad 0.00057919]$$

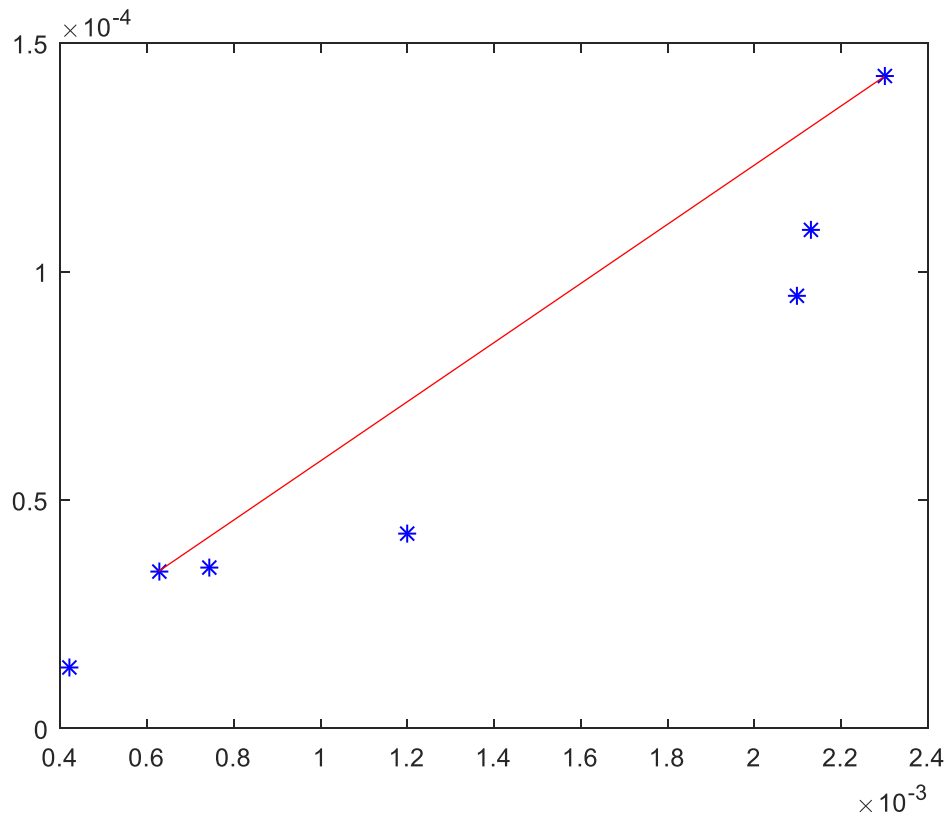$$Y = 10^{-4}.\,[0.55001, \qquad 0.40168, \qquad 0.24558]$$
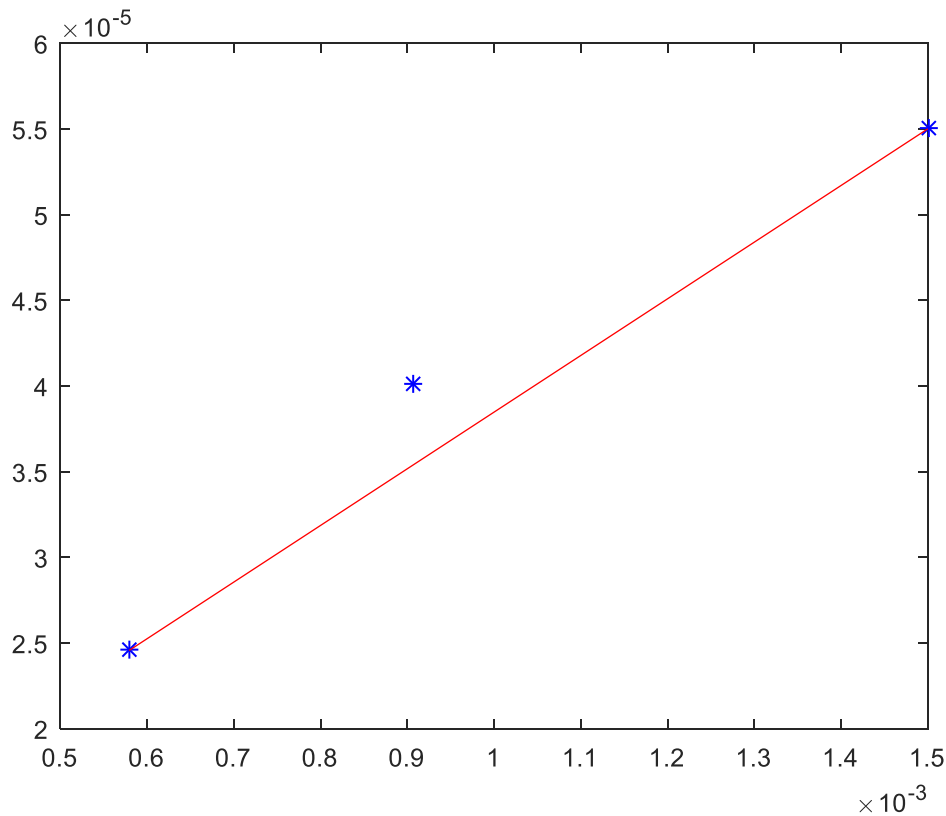
Figure III.7: Calculation of the mean crystalline size and micro deformation for pure Fe powder.

The calculated points serve to trace a right line for which:

- the slope worth's: $a = 0.0331$
- the ordered at the origin value is: $b = 0.00000054093$

Which allow to:

- a calculated mean grain size of: $d = 30.2470$ nm
- a calculated micro- deformations percentage of: $\varepsilon = 0.47\%$.

- **for MA Fe$_{40}$Co$_{60}$ powder (2h milling)**

Localized diffraction angles (diffractometer data in degrees):

$$2\theta = [44.933, \quad 65.859, \quad 82.55]$$

$$X = 10^{-4}.\,[35.913, 14.651, 6.6731]$$

$$Y = 10^{-5}.[31.711, 10.68, 3.2631]$$

Figure III.8: Calculation of the mean crystalline size and micro deformationfor MA Fe$_{40}$Co$_{60}$ powder (2h milling).

The calculated points serve to trace a right line for which:

- the slope worth's: $a = 0.0973$
- the ordered at the origin value is: $b = 0.000032293$

Which allow to:

- a calculated mean grain size of: $d = 10.2784$ nm
- a calculated micro- deformations percentage of: $\varepsilon = 1.14\%$.

- **for MA Fe$_{40}$Co$_{60}$ powder (8h milling)**

Localized diffraction angles (diffractometer data in degrees):

$$2\theta = [44.818, \ 82.415]$$

$$X = 10^{-4}.[38.581, 7.0742]$$

$$Y = 10^{-5}.[36.42\ ,3.6573]$$

Figure III.9: Calculation of the mean crystalline size and micro deformationfor MA Fe$_{40}$Co$_{60}$ powder (8h milling).

The calculated points serve to trace a right line for which:

- the slope worth's: $a = 0.1040$

- the ordered at the origin value is: $b = 0.000036989$

Which allow to:

- a calculated mean grain size of: $d = 9.6167$ nm

- a calculated micro- deformations percentage of: $\varepsilon = 1.22\%$.

- **for MA Fe$_{40}$Co$_{60}$ powder (12h milling)**

Localized diffraction angles (diffractometer data in degrees):

$$2\theta = [44.753,\ \ 64.914,\ \ 82.216]$$

$$X = 10^{-4}.[40.736,\quad 6.1862,\quad 8.2427\ ]$$

$$Y = 10^{-5}.\,[40.492, \qquad 1.8558, \qquad 4.9456]$$

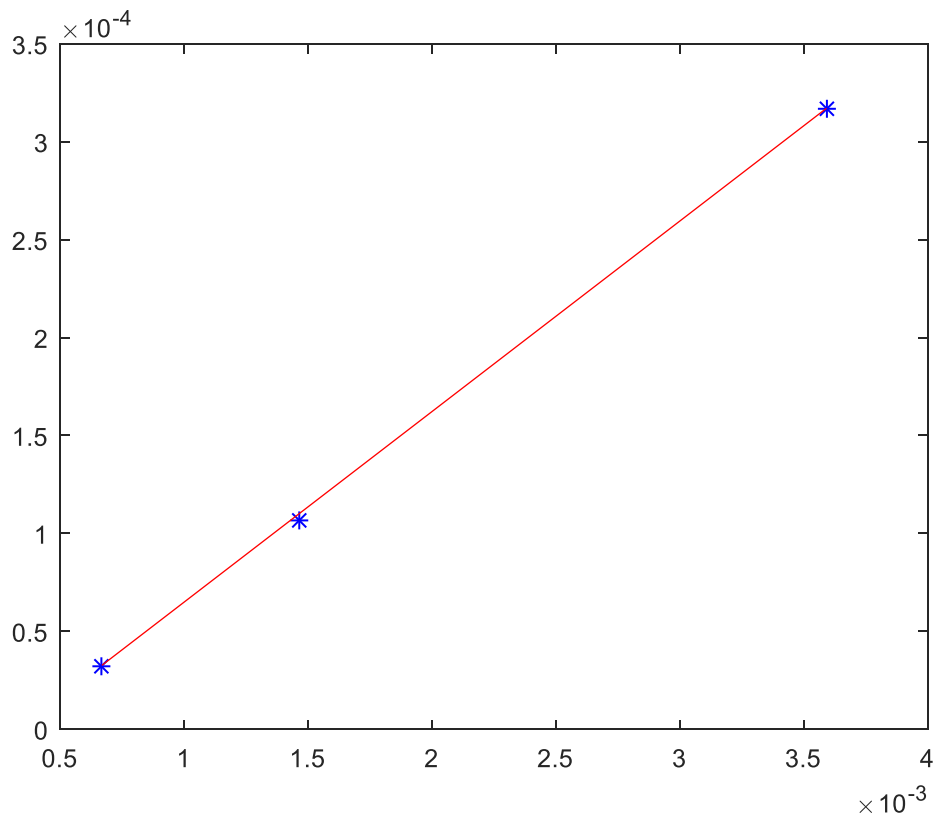**Figure III.10: Calculation of the mean crystalline size and micro deformationfor MA Fe₄₀Co₆₀ powder (12h milling).**

The calculated points serve to trace a right line for which:

-   the slope worth's: $a = 0.1118$
-   the ordered at the origin value is: $b = 0.000050621$

Which allow to:

-   a calculated mean grain size of: $d = 8.9423$ nm
-   a calculated micro- deformations percentage of: $\varepsilon = 1.42\%$.

- **for MA Fe₄₀Co₆₀ powder (36h milling)**

Localized diffraction angles (diffractometer data in degrees):

$$2\theta = [44.64, \ 65.034, \qquad 82.058 \ 82.721]$$

$$X = .\,10^{-3}[4.3\,, \qquad 1.7\,, \qquad 0.54401\,, 0.8806 \quad]$$

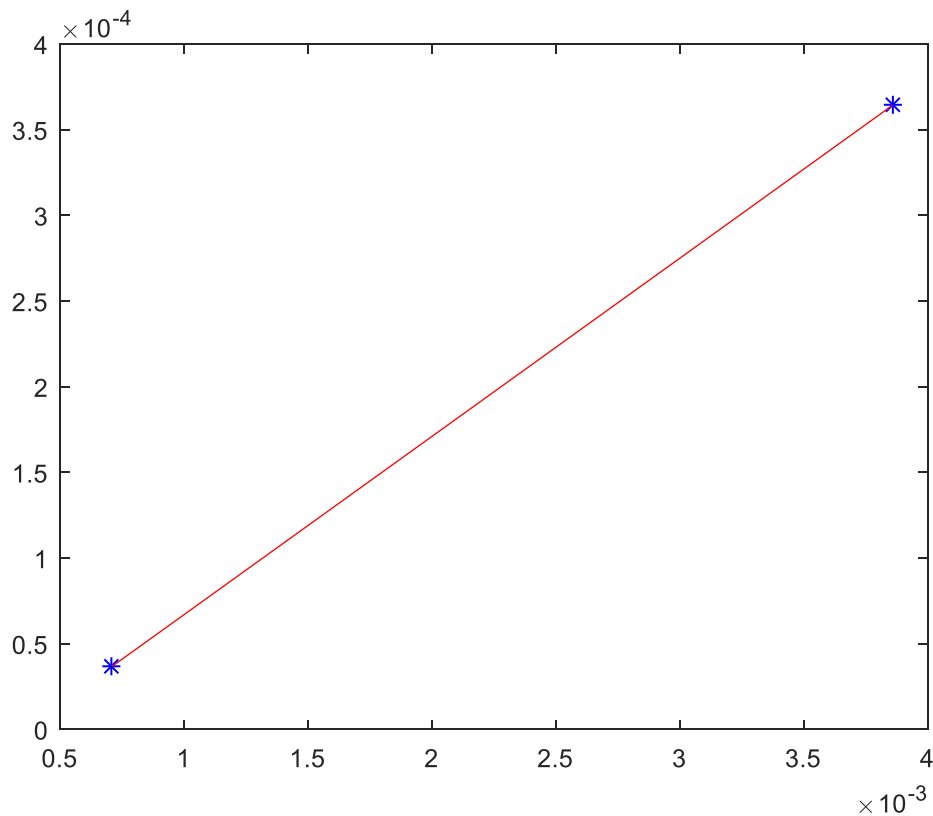$$Y = 10^{-5}.\,[44.796, \qquad 13.921\,, 2.2, \qquad 5.6272]$$

Figure III.11: Calculation of the mean crystalline size and micro deformationfor MA Fe$_{40}$Co$_{60}$ powder (36h milling).

The calculated points serve to trace a right line for which:

- the slope worth's: $a = 0.1145$

- the ordered at the origin value is: $b = 0.0000446$

Which allow to:

- a calculated mean grain size of: $d = 8.7299$ nm

- a calculated micro- deformations percentage of: $\varepsilon = 1.34\%$.

- **for MA Fe$_{40}$Co$_{60}$ powder (60h milling)**

Localized diffraction angles (diffractometer data in degrees):

$$2\theta = [44.66,\ 65.071,\ 82.351]$$

$$X = 10^{-4}.\left[\,43.61,\quad 9.1368\,,2.8086\ \right]$$

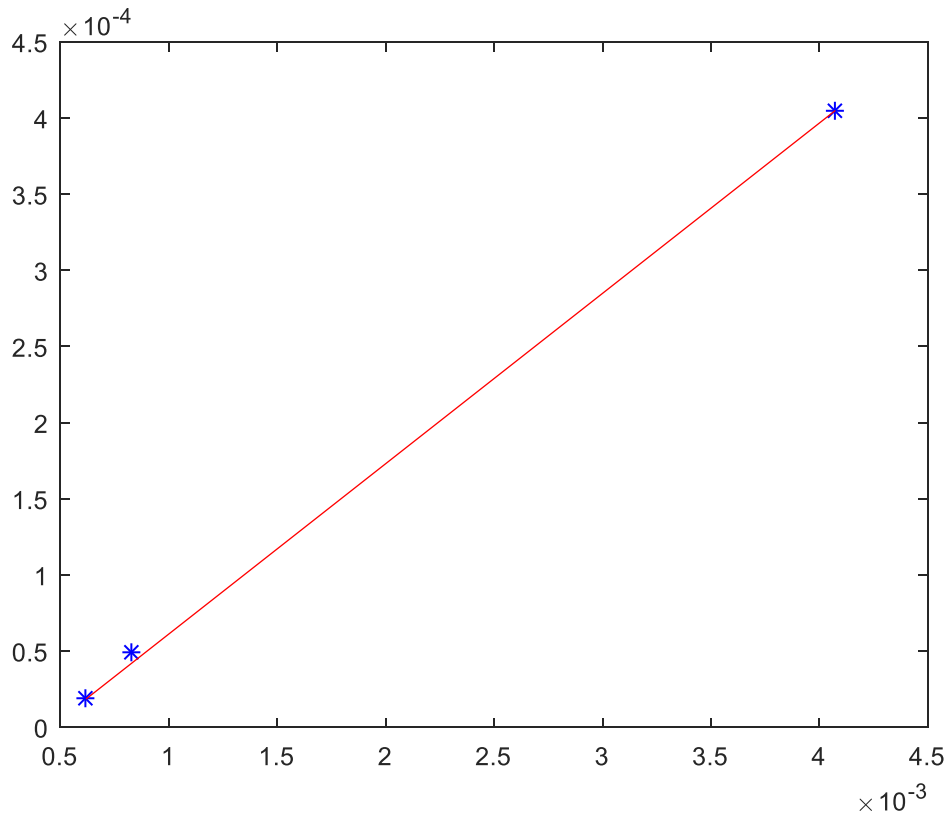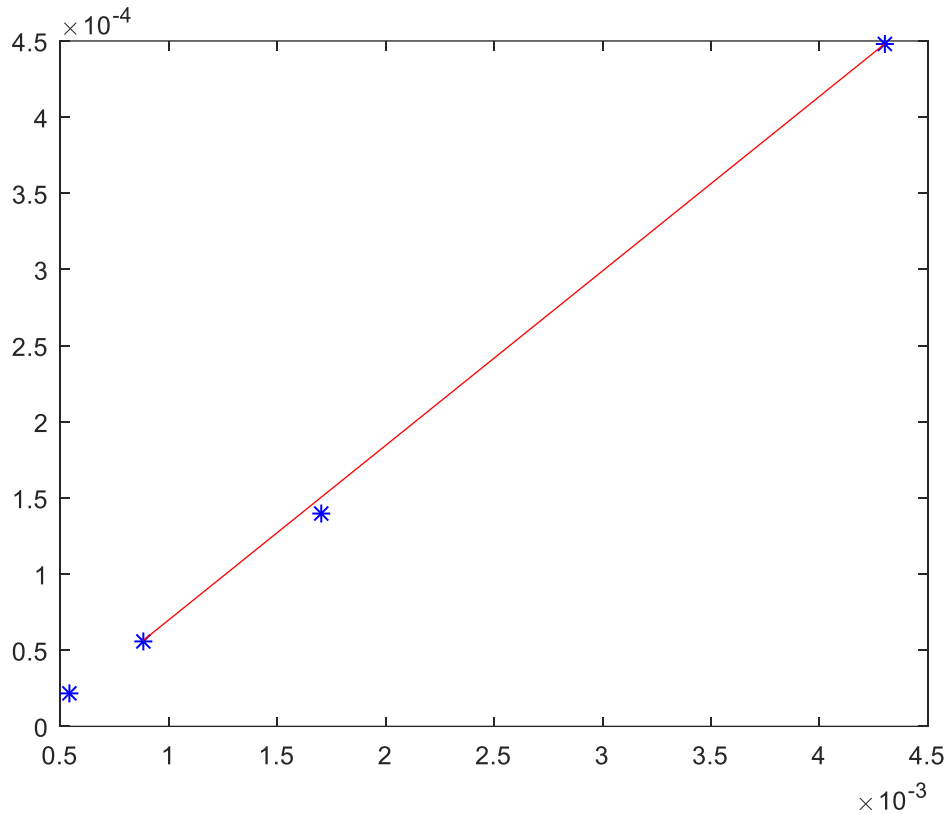$$Y = 10^{-6}.\left[\,462\,,\ 40.8\,,\ 5.7577\ \right]$$
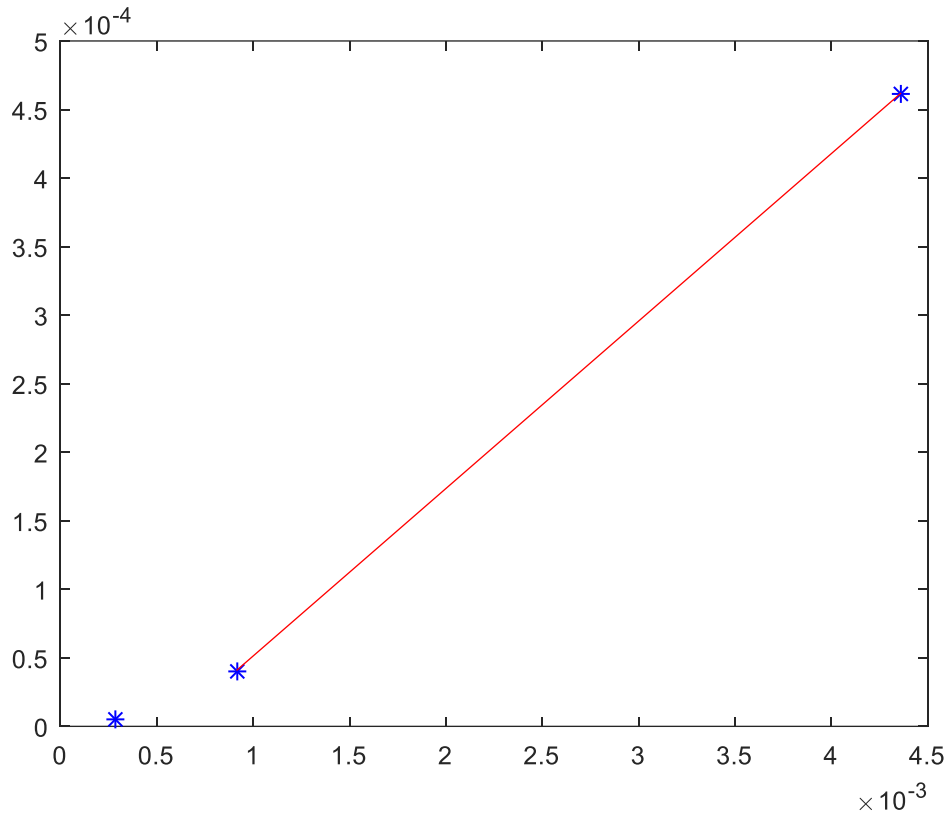
Figure III.12: Calculation of the mean crystalline size and micro deformationfor MA Fe₄₀Co₆₀ powder (60h milling).

The calculated points serve to trace a right line for which:

-   the slope worth's: $a = 0.1222$
-   the ordered at the origin value is: $b = 0.000070835$

Which allow to:

-   a calculated mean grain size of: $d = 8.1845$ nm
-   a calculated micro- deformations percentage of: $\varepsilon = 1.68\%$.

Fig. III.13 shows the grain size refinement. Before milling the average grain size is $d(Fe) \approx 30.247 nm$ with corresponding residual micro- deformations of 0.47% and $d(Co) \approx 15.4517 nm$ with corresponding residual micro- deformations of 0.5%. The average grain size adopts a decrease evolution with milling progression to reach 8.1845nm after 60h milling. Simultaneously, the residual micro-deformations percentage increases to a highest fraction of 1.68% due to severe plastic deformations accumulated during high- energy ball milling.
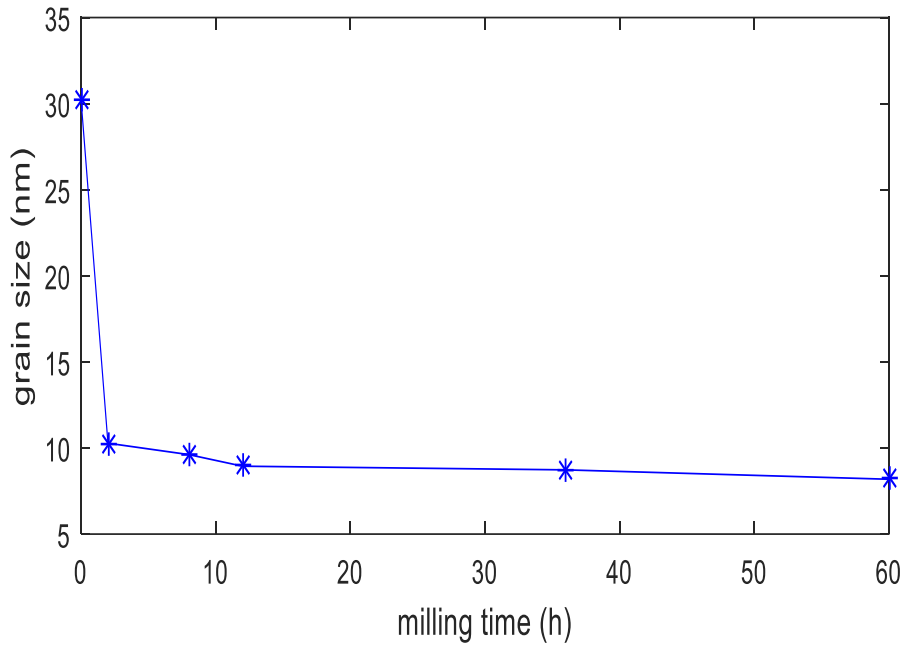
Figure III.13: Grain size refinement according to milling duration.
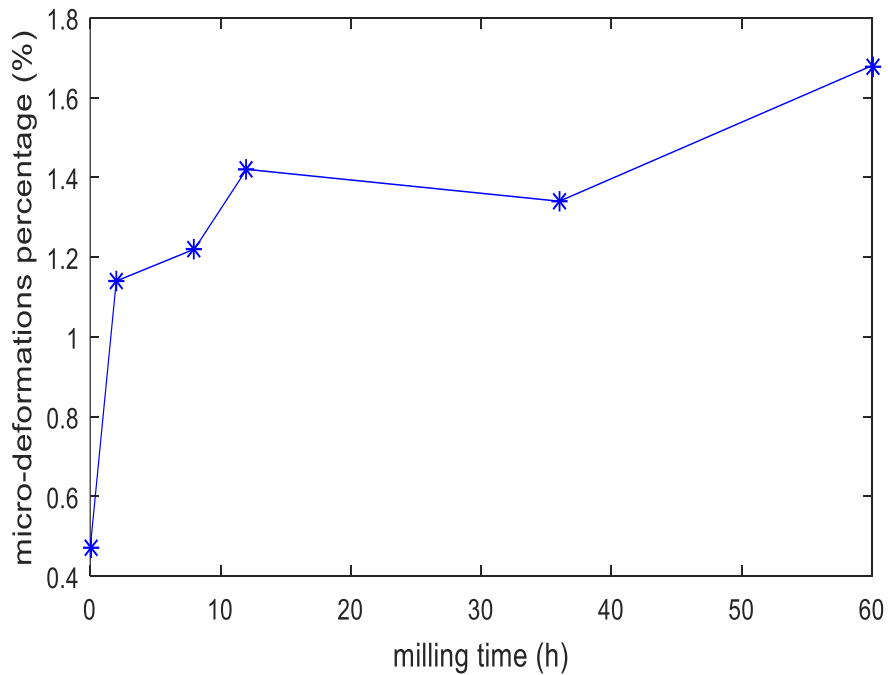
Figure III.14: Residual micro deformation according to milling duration.

III.3 SEM Characterization

The powder's morphology and particles size are observed by a scanning electron microscope (JEOL JSM 6360). The technique is to stick the powders samples on polished supports covered with resin and achieve micrographs of 100 to 2000 enlargements.

First morphology observation Fig III.15.a of the elemental Fe powder manifests a dendrite aspect of powder with coarse particles size (around $100\mu m$). After 2h of milling, there are different particles sizes in the assembly. This difference is linked to the fraction-welding mechanisms introduced by high- energy mechanical alloying. In Fig III.15.b the fracture- welding mechanism is illustrated in a magnified micrograph (2000 times). With milling progression, the mechanism is more important due to collisions between the balls and the container's walls and leads to flattened angular shapes of particles FigIII.15.c with complete disappearance of the dendrite aspect. Prolonged ball milling to 60h Fig III.15.d results in larger agglomerations of homogeneous particles of less than 10 μm sizes.
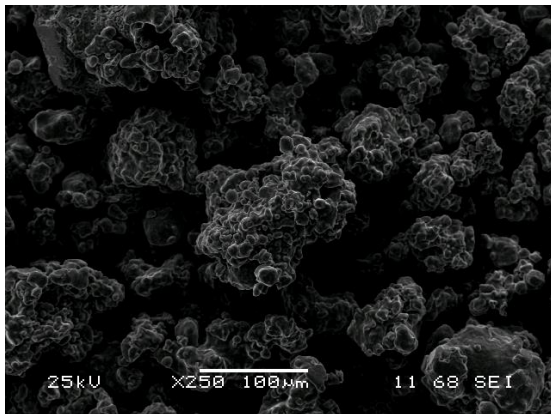
Figure III.15.a : Elemental Fe micrograph
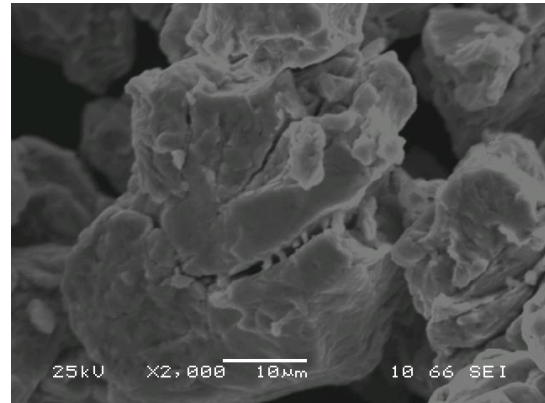
Figure III.15.b :MA Fe$_{40}$Co$_{60}$ micrograph (2h milling : fracture phenomenon)
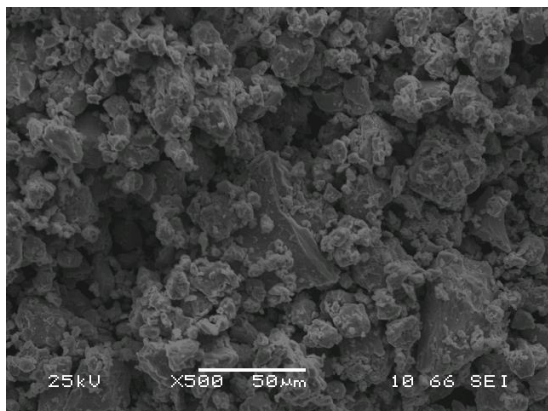
Figure III.15.c: MA Fe$_{40}$Co$_{60}$ micrograph (12h milling)
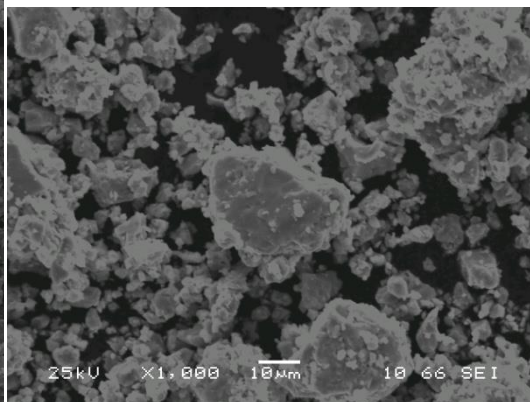
Figure III.15.d: MA Fe$_{40}$Co$_{60}$ micrograph (60h milling)

Finally, Fig.III.15.e we show the inconvenient of the home made test samples, which affects dispersion quality of the nanocrystalline Fe powders into the resin matrix. Ultrasound assisted stirring is required for better dispersion of the nanocrystalline powders into the resin matrix in order to avoid inhomogenous mixtures.
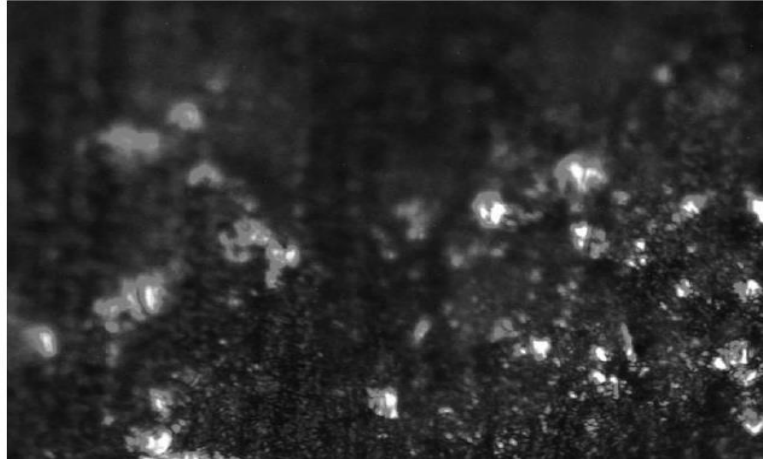
FigureIII.15.e: SEM micrograph of Fe-Co based nanocomposites (36 milling).

Conclusion

In this chapter, we describe the elaboration process and structural characterization conducted for the test samples. It can be summed up in three steps: elaborations of the nano-fillers (nanocrystalline $Fe_{40}Co_{60}$ powders) by mechanical alloying (MA) technique, structural XRD analysis and morphological observation via scanning electron microscopy (SEM). Obtained results confirm the formation of the $Fe_{40}Co_{60}$alloy at the solid state, the grain size refinement and the increase of micro-deformations percentage during mechanical alloying. The microscopy observation illustrates the powder's morphology changes and the particles size refinement.

Chapter IV   Electromagnetic characterization

Introduction

For the electromagnetic characterization, bulk samples of the Fe-Co based nanocomposites were shaped in a home moulder by dispersion of coarse Fe, and MA $Fe_{40}Co_{60}$in a continuous matrix of commercial epoxy resin. The obtained bulk samples match the metallic X-band wave-guide (R100) dimensions used for electromagnetic characterization. The two-port S_{ij} scattering parameters were measured via an Agilent 8791 ES network analyzer.This characterization took place in stages:

- Measurement of parameters in an X-band waveguide associated with a network analyzer. Both empty and under load measurements were taken,

- Implementation of the Nicolson-Ross-Weir algorithm using Matlab software for the extraction of permittivity and permeability relative to the elaborated materials,

- Determination of the relative permittivity and permeability of the empty wave-guide,

- Determination of the electric and magnetic losses relative to the elaborated materials.

IV.1 S-Parameters Measurement

Electromagnetic characterization is accomplished in terms of relative dielectric permittivity and relative magnetic permeability using the transmission/reflection technique. Measuring cell consists of a section of the metallic rectangular wave-guide R100 filled with the sample to be characterized. The S_{ij} parameters measurements were accomplished by sandwiching a bulk sample between two rectangular waveguides connected to the two ports of the VNA so that it is perpendicular to the direction of the electromagnetic wave propagation. After calibration, the S_{ij} spectra were recorded on the VNA as responses of the sample over the X-band (8.2 – 12.4 GHz).
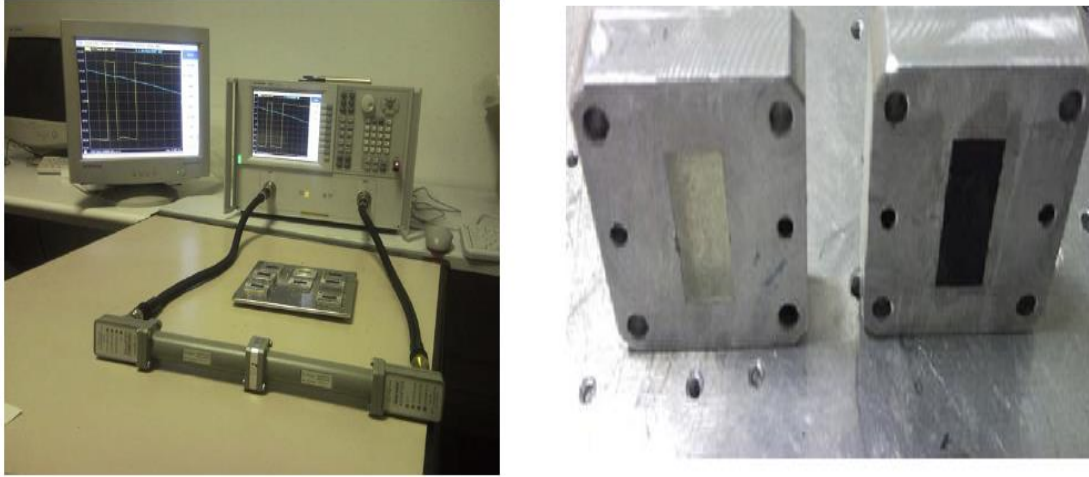
Figure IV.1: S parameters measurements cell.

In this part of the work, we consider four measures of dispersion matrix S; two composite samples of different compositions were placed in the rectangular section of the waveguide associated with a network analyzer for measuring S parameters. The 2 samples differ in their compositions. We considered a composite sample of epoxy resin alone and one pure iron composite sample including the measurement of the waveguide in vacuum. The spectra of the Sij parameters are drawn up as follows according to the frequency range corresponding to the waveguide's bandwidth.

IV.2 Results and discussion

II.2.1 Empty measure

For the VNA device, the empty measure is a fundamental step for calibration. In this section, we comment the recorded S parameter's module spectra showed in figure IV.2.
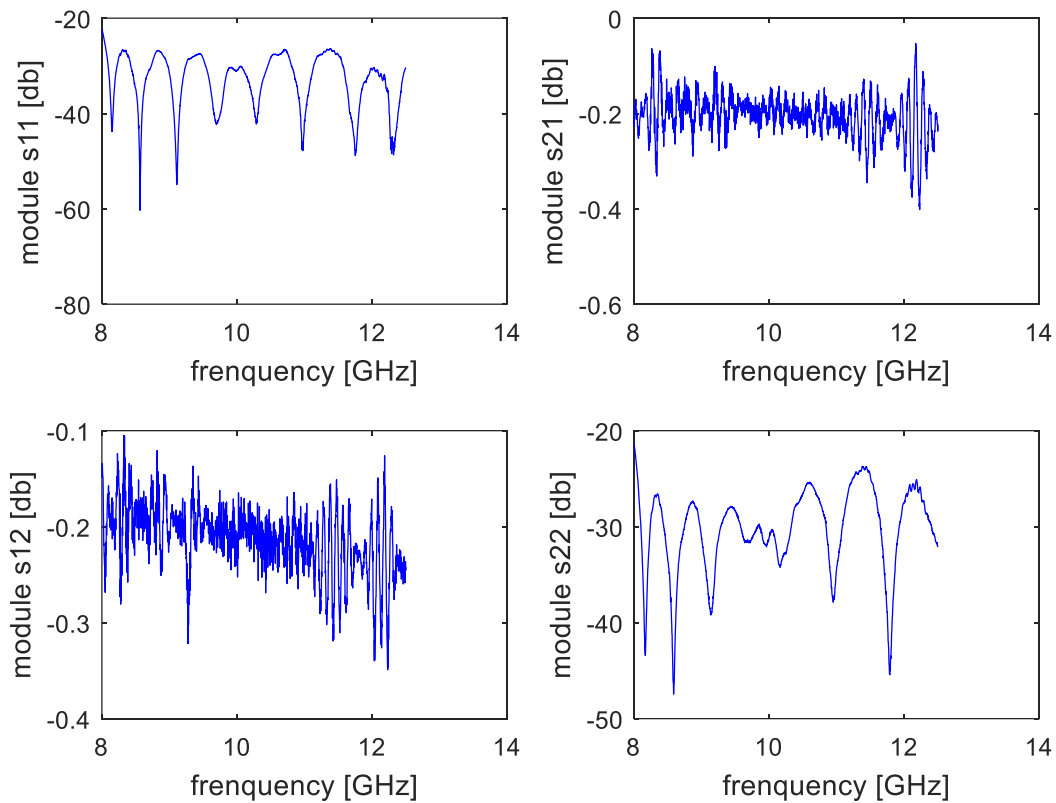
Figure IV.2: S parameters spectra of the empty wave-guide.

→ **S11 and S22 parameters**

From these graphs, which represent the reflection intensity at port 1 and port 2 respectively as function of frequency, it is found that the vacuum (air medium inside the wave-guide) has a low module reflection (almost no reflection). Over the frequency band, S11module varies between -25 dB and -50 dB while S22module varies between -20 dB and -45 dB.

→ **S12 and S21 parameters**

According to the S12 and S21 modules shown in the graph, it is directly apparent that the vacuum has near-zero 0dB transmission modules. It is concluded that in the presence of vacuum the transmission EM energy is excellent (about 96% of this energy)

- **Electromagnetic parameters**

Extracted electromagnetic parameters spectra (both dielectric permittivity and magnetic permeability of the empty wave- guide)via the NRW algorithm are shown in figure IV.3. .
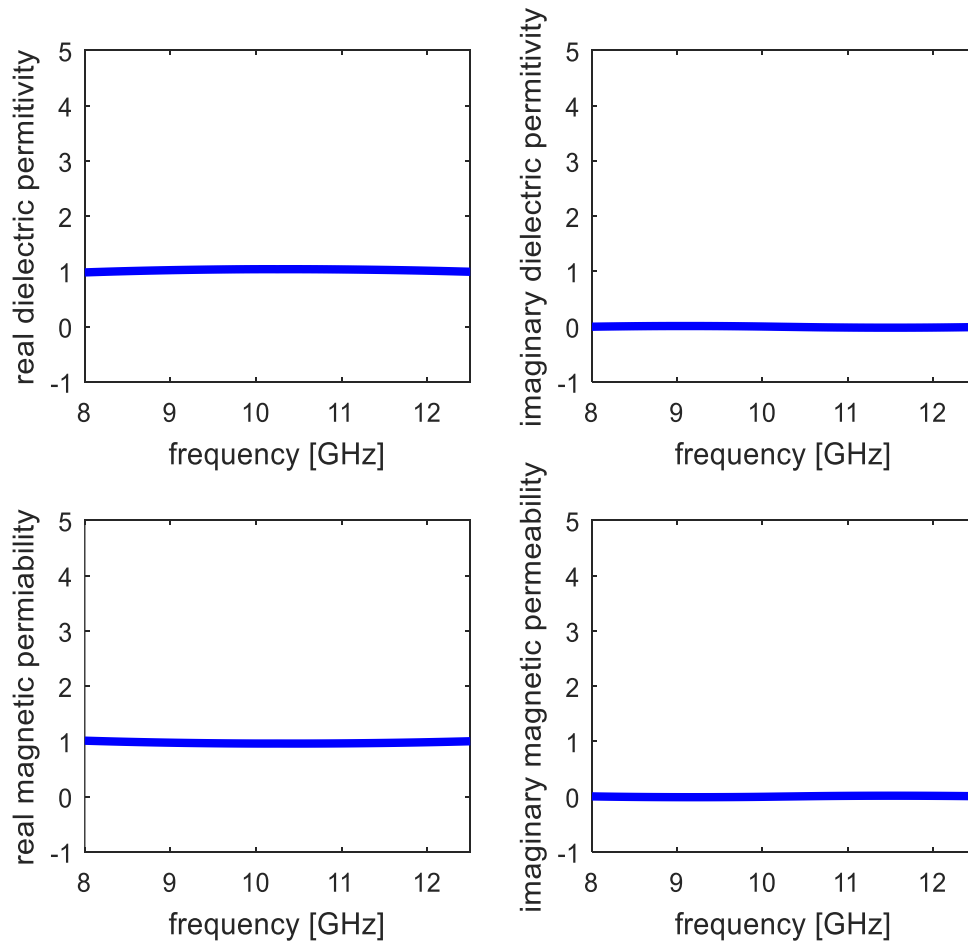
Figure IV.3 Electromagnetic parameters spectra of the empty wave-guide.

From these graphs, we find the real part of the relative permittivity of air, which is almost constant with a fluctuation around one same as the spectra of the real portion of the relative permeability shown. In addition, we see that the imaginary part of the relative permittivity (εr") of air is fluctuating around zero and the imaginary part of the relative permeability (μr") of air is very weak expressing the non-magnetic character of the media.

Consequently, the losses tangent spectra (both electric and magnetic) corresponding to the wave-guide at vacuum are represented in figure IV.4. These figures show that the empty wave- guide has low dielectric and magnetic losses ($tan\delta_E \cong 0$ and $tan\delta_M \cong 0$).
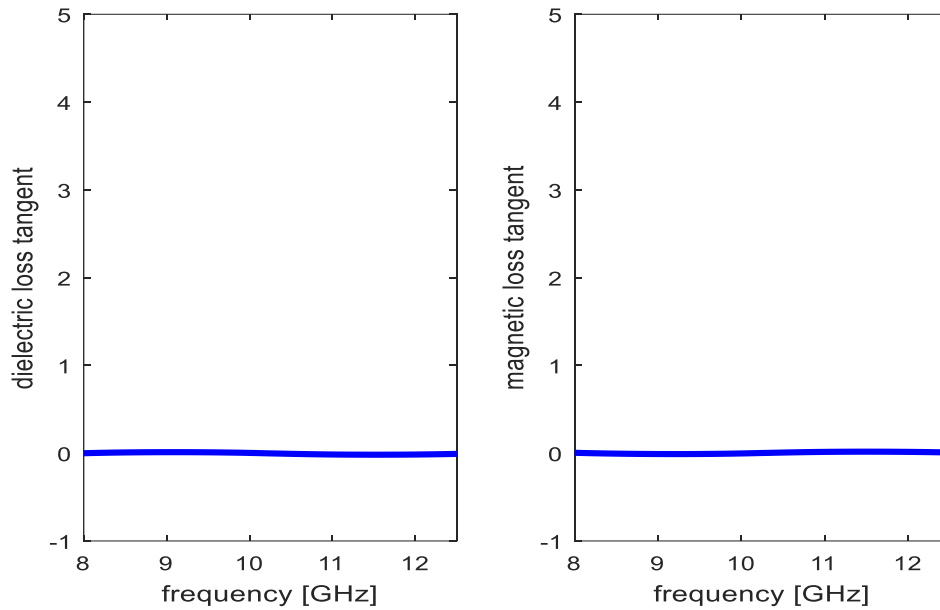
Figure IV.4Electric and magnetic losses tangent spectra of the empty wave-guide.

IV.2. Filled wave-guide

For the filled wave-guide experiment, pure epoxy resin and pure Fe samples test are considered. After VNA measurement, the corresponding reordered S parameters module spectra are superimposed in figure IV.5.

→ S11 and S22 parameters

These graphs show that the presence ofother materials mediums in the experiment increases the reflection modules S11 and S22 and makes them more important. As it can be seen, the S_{11}module and the S_{22} are varying between (-4 dB and -15 dB). The reflection is more important for the Fe sample. This difference is linked to the conductor character of the Fe powder incrusted in the epoxy resin matrix.

S12 and S21 parameters

The corresponding graphs show that presence of any material or substance in the waveguide weakens the transmission coefficient module. The resin and pure iron havemuch lower transmission modules compared to air. High transmission coefficient value are observed for epoxy resin sample compared to coarse Fe based sample. We conclude that the transmitted EM energy in the presence of another medium is low compared to air.
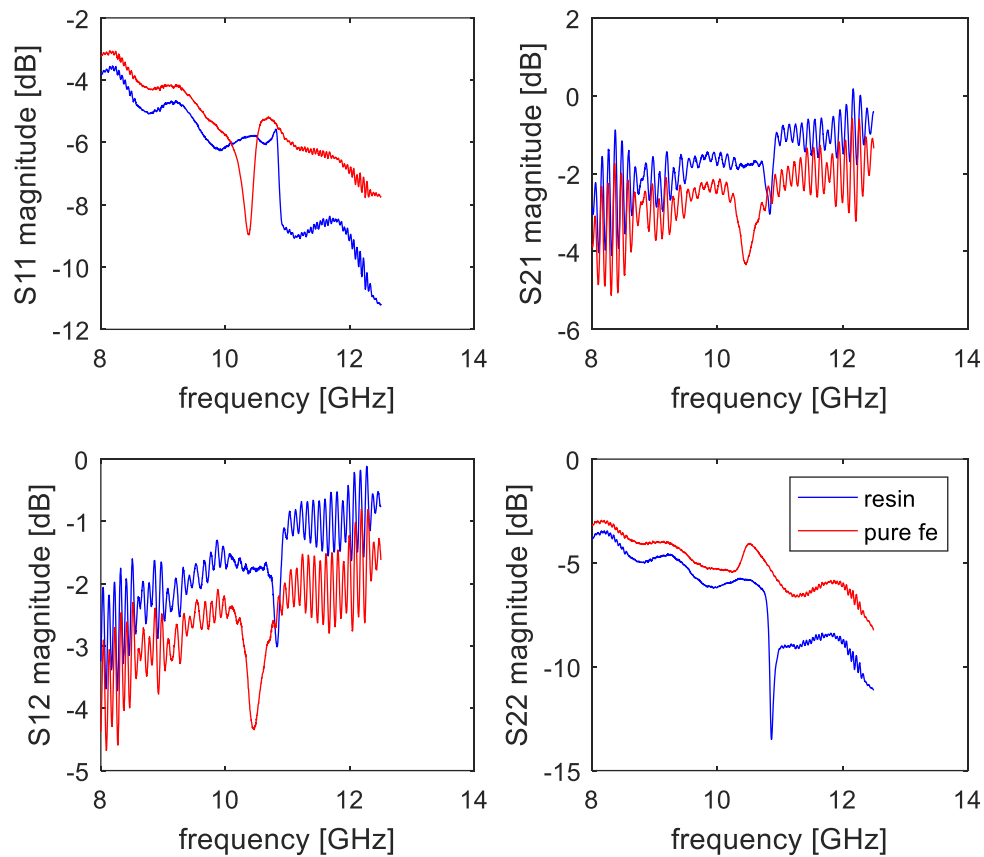
Figure IV.5: Superimposed S parameters spectra ofepoxy resin matrix and Fe samples.

Epoxy resin electromagnetic parameters

The obtained spectra for the relative dielectric permittivity $\varepsilon_r = \varepsilon_r' - j\varepsilon_r''$, the relative magnetic permeability $\mu_r = \mu_r' - j\mu_r''$, and the corresponding dielectric loss tangent $\tan\delta_E = \frac{\varepsilon_r''}{\varepsilon_r'}$ and magnetic loss tangent $\tan\delta_M = \frac{\mu_r''}{\mu_r'}$ are illustrated in Fig.IV.6. As we can observe, the introduction of a different material medium inside the wave- guide induce new S parameters. Consequently, the extracted electromagnetic parameters change. The epoxy resin matrix show a real dielectric permittivity constant fluctuating around 3, which is a known value for the epoxy resin (cited in bibliography). Dielectric permittivity originates from the space charge polarization as a response to the action of the electromagnetic field. It is clear that the epoxy resin medium is more reactive with the electric field compared to air. Whereas the imaginary dielectric permittivity spectrum expressing the dielectric loss in the medium exhibit low values over the X- band and fluctuate around zero.

.
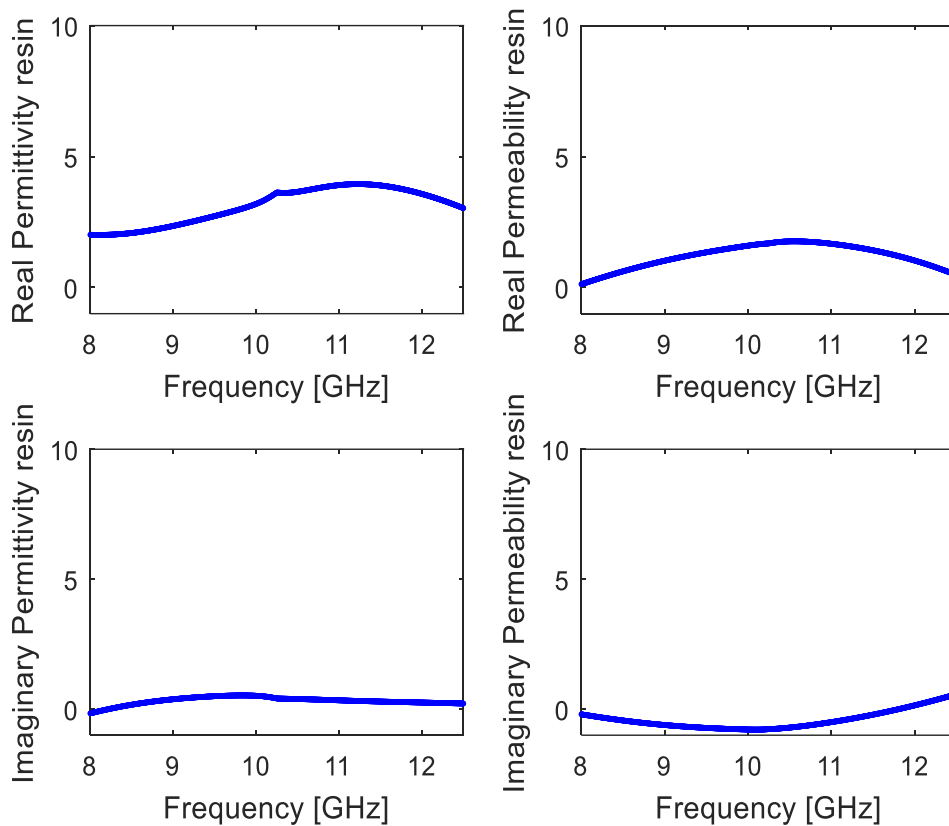
Figure IV.6: Electromagnetic parameters spectra of epoxy resin sample test.

The spectra of real part of relative magnetic permeability corresponding to resin shows almost constant behavior around 1 giving information about the non-magnetic nature of the resin. Consequently, the imaginary magnetic permeability has trend to fluctuate around zero.

The electric and magnetic losses tangent spectra corresponding to the epoxy resin sample are represented in Fig.IV.7. The material medium is low dielectric and magnetic losses over the X-band with fluctuated spectra around zero values.
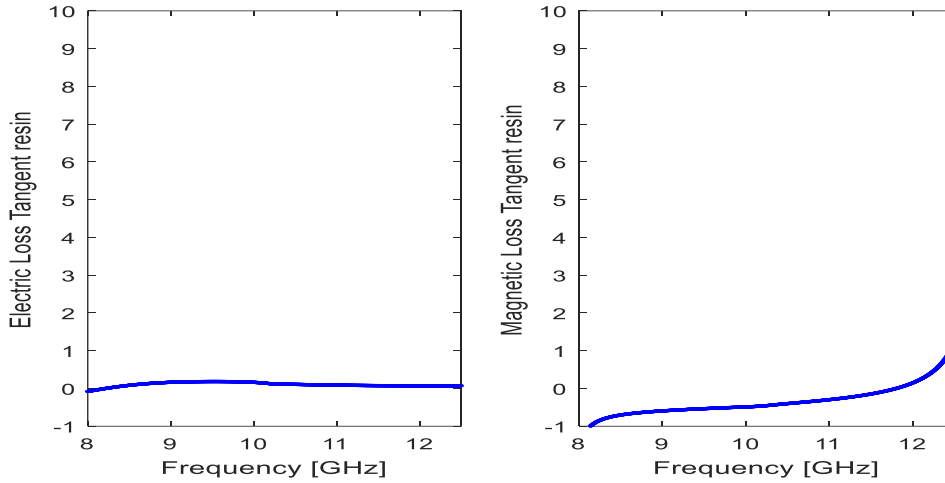
Figure IV.7: Electric and magnetic losses tangent spectra of epoxy resin sample test.

Fe electromagnetic parameters

Fig IV.8 illustrates the real and imaginary parts of the relative dielectric permittivity and magnetic permeability versus frequency corresponding to the prepared Fe based composite. Important dielectric permittivity constants (real parts) are due to metallic types of the filler. Dielectric permittivity originates from the space charge polarization as a response to the action of the electromagnetic field. The variation of the magnetic permeability is more noticeable compared to that of the dielectric permittivity. By looking at the microwave parameters spectra, one can note the contribution of the Fe powder to improve the dielectric loss tangent $(tg\delta_E = \frac{\varepsilon_r''}{\varepsilon_r'})$ and magnetic loss tangent $(tg\delta_M = \frac{\mu_r''}{\mu_r'})$ depicted in Fig IV.9, specially the magnetic loss tangent due to the superior magnetic properties of Fe.
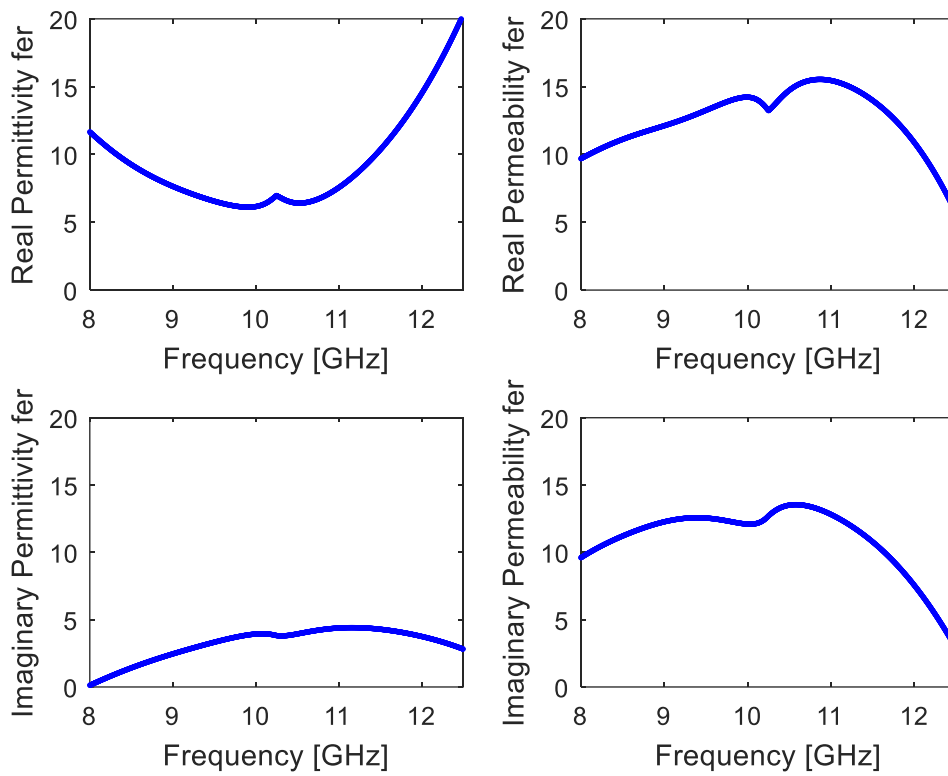
Figure IV.8: Electromagnetic parameters spectra of Fe based composite sample test.
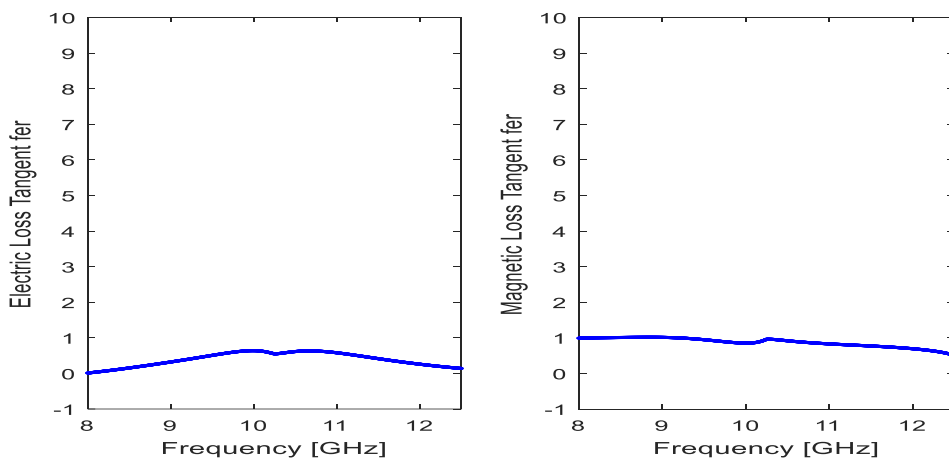
Figure IV.9: Electric and magnetic losses tangent spectra of Fe based composite sample test.

```
        ┌─────────────────────┐
        │   Setup Vector      │
        │  Network Analyzer   │
        └─────────────────────┘
                  │
                  ▼
        ┌─────────────────────┐
        │    Setting the      │
        │ Frequency range/    │
        │ Number of points    │
        └─────────────────────┘
                  │
                  ▼
        ┌─────────────────────┐
        │ Define Sample holder│
        │ and sample parameters│
        │ (eg. length,cutoff  │
        │ frequencies,etc. )  │
        └─────────────────────┘
                  │
                  ▼
        ┌─────────────────────┐
        │  Calibrate system   │
        │ using Full 2-port/  │
        │ One path 2-port/    │
        │ Full one port       │
        │ calibrations        │
        └─────────────────────┘
                  │
                  ▼
        ┌─────────────────────┐
        │   Place MUT on      │
        │     fixture         │
        └─────────────────────┘
                  │
                  ▼
        ┌─────────────────────┐
        │     Measure         │
        │   S-parameter       │
        └─────────────────────┘
                  │
                  ▼
        ┌─────────────────────┐
        │ Perform calculation │
        └─────────────────────┘
                  │
                  ▼
        ┌─────────────────────┐
        │  Display complex    │
        │   permittivity/     │
        │   permeability      │
        └─────────────────────┘
                  │
                  ▼
        ┌─────────────────────┐
        │        End          │
        └─────────────────────┘
```
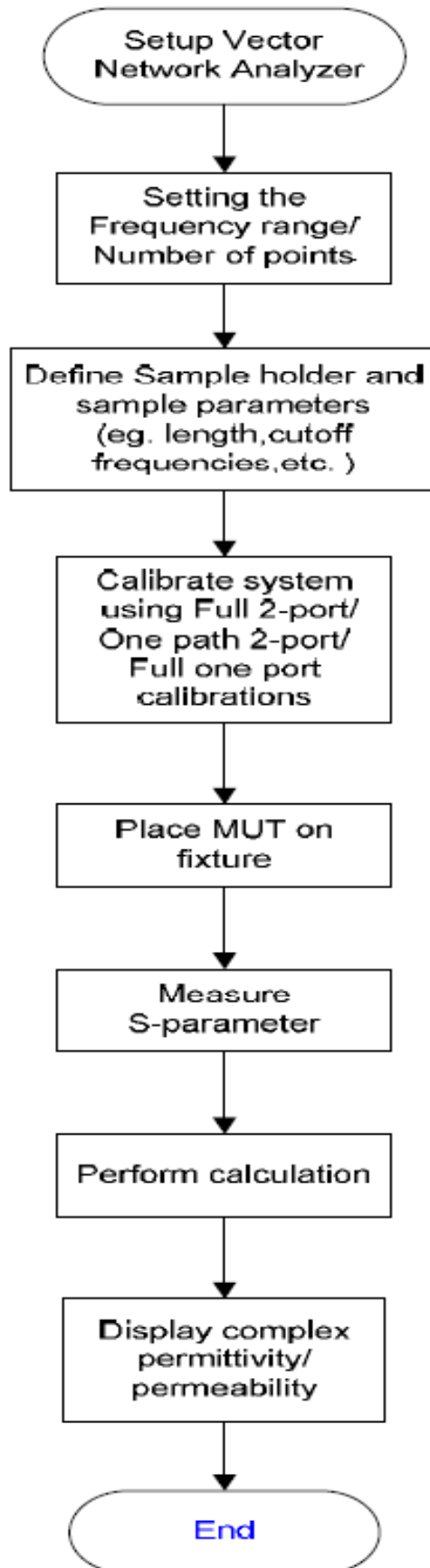
Nicholson Ross Weir
mathematical model

Use following S-
parameters:
$S11, S21, S12, S22$

Calculate Reflection
Coefficient, Γ

Calculate
Transmission
Coefficient , T

*Calculation is correct with
the condition* $|\Gamma| < 1$

Calculate
permeability, μ

Calculate
permittivity, ε

*Calculation is done in real
and imaginary terms*

End
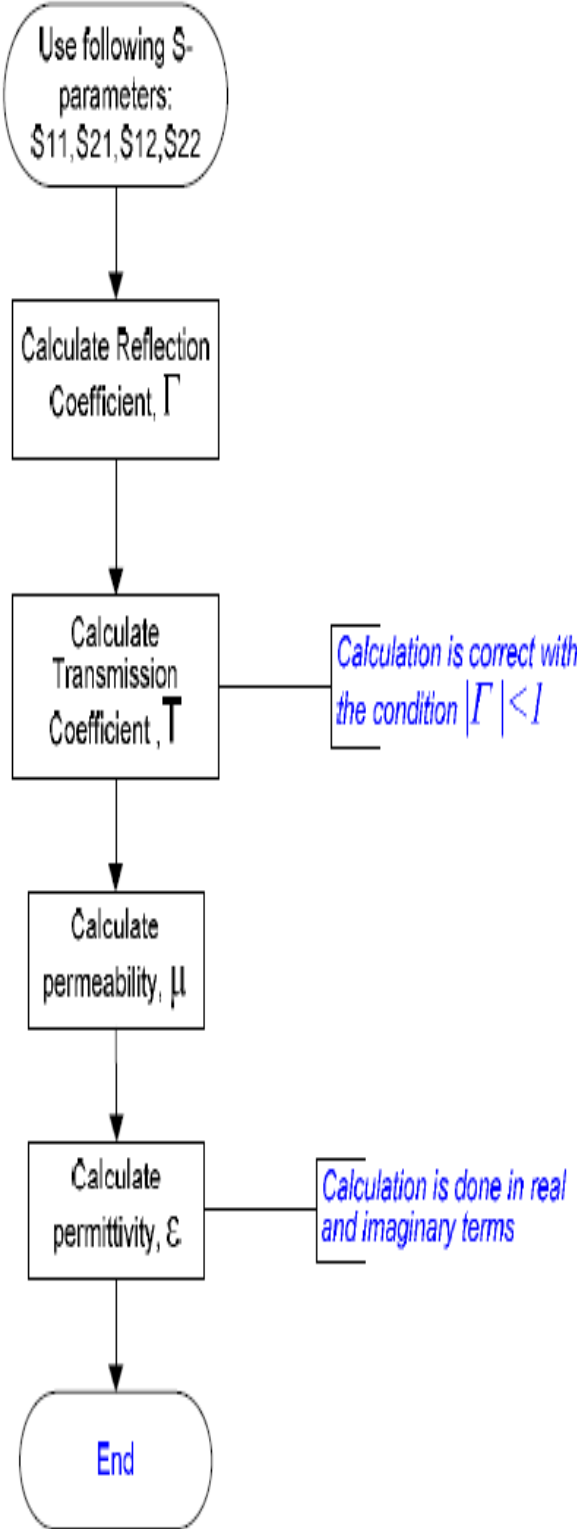
General Conclusion

The main objective of the use of coating in aircraft industry is to minimize the effect of corrosion and wear in the components integrity. Otherwise, in such responsible and expensive equipment these issues lead to a failure that causes serious safety and economic effects. This work was carried out with the aim of making known the characteristics of a nanostructured material for aircraft coatings.

The choice of constituent materials plays a dominant role. This led us to give an idea about the materials composites that can be used for aircraft coating. With the advent of nanomaterials, choices are multiplying and are moving towards nanocomposites to allow the aeronautics industry to benefit from the new properties of nanomaterials.

Mechanical alloying (ball milling) technique can lead the materials to the nanoscale dimension. The structural characterization through powder X-Ray Diffraction analysis via the Halder- Wagner theory and the Scanning Electron Microscopy (SEM) show the original properties of the obtained nanomaterials. Elaborated nanomaterials serve as fillers to produce nanocomposites.

To study the behavior of the nanocomposites subjected to the action of an electromagnetic wave in a microwave band, it is necessary to characterize the electromagnetic properties of the material in terms of dielectric permittivity and magnetic permeability.The choice of the characterization method, the size and shape of the available test sample, the equipment and the frequency band are closely related.

In this study we have opted for a transmission/reflection technique that was accomplished using a rectangular metallic waveguide in combination with a network analyzer.The dielectric permittivity as well as the relative magnetic permeability of the shaped test samples was extracted in Matlab using the Nicolson-Ross-Weir algorithm.

The general remarks that can be highlighted after the completion of this work are as follows:

- The production of nanostructed Fe-Co powders by the severe plastic deformation (mechanical alloying) in order to observe their properties at the nanoscale,

- The obtained nanocomposites samples by incorporating of the nanostructured Fe-Co alloy in an epoxy resin matrix through the solution dispersion process,

- X-ray diffraction technique that serves in the characterization of the nanocrystalline powders provides information on structures by studying the different spectra obtained by XRD diffractometer,

- Halder wagner method links the grain size and the accumulated micro-deformations in the crystalline structure by a right equation which allow us to observe their evolution to different time of milling,

- Scanning electron microscopy allows the observations of nanomaterials surfaces by the presentation of their morphology,

- The use of the network analyzer allowed us to characterize over a large frequency range. The X band being a very rich band in most applications.

- The electromagnetic characterization uses advanced microwave equipment such as the metallic waveguide and the network analyzer,

- The NRW routine of calculating the spectra of the dielectric permittivity and the magnetic permeability allowed us to reinforce our exercise of the Matlab software, to verify the problems of this method and to try to provide solutions.

The perspectives that can be derived from this work can be summarized in:

- Extraction of dielectric permittivity and permeability spectra by numerical methods.

- Expand the study for other frequency bands, which will require more sample forms (other processing techniques) and other methods of electromagnetic characterization

-study the behavior of the same material but in terms of its relation to the exterior transmitted or emitted signals to and from the aircraft

Bibliografic references

[1] J. Lince, Coatings for Aerospace Applications, International Conference on Metallurgical Coatings and Thin Films, California (2017).

[2] I. Obieta, J. Marcos, Nanomaterials: Opportunities and Challenges for Aerospace, Meeting Proceedings RTO-MP-AVT 122, Spain (2005) pp.1-10.

[3] J. Musil, Surf. Coat. Technol. 322 (2000) p.125.

[4] P. Holubar, M. Jilek, M. Sima, Surf. Coat.Technol. 145 (2000)pp. 133-134

[5] S. Veprek, S. Reiprich, Thin Solid Films 64 (1995) pp. 268

[6] A.A. Voevodin, J.S. Zabinski; Thin Solid Films 370 (2000) 223-231

[7] P.H. Mayrhofer, C. Mitterer ; Surf. Coat. Technol. 133/134 (2000) 131

[8] M. Misina, J. Musil, S. Kadlec, Surf. Coat.Technol. 110 (1998) 168

[9] J. Musil, H. Polakova, Surf. Coat, Technol. 127 (2000) 99

[10] Shaw et al, The dependency of microstructure and properties of nanostructured coatings onplasma spray conditions, Surf. CoatingTechnol, 2000, 130-180

[11] C. Zhou et al, J. EurCeram.Soc, 2003, 23, 1449

[12] P. Christian, F. Von der Kammer, M. Baalousha, et Th. Hofmann, « Nanoparticules: structure, properties, preparation and behaviour in environmental media », Ecotoxicology

[13]P. Heeraet S. Shanmugam, « Nanoparticle Characterization and Application: An Overview », p. 8, 2015.

 [14] H. Dai, « Carbon Nanotubes: Synthesis, Integration, and Properties », Acc. Chem.

[15] A. Kazemzadeh, M. A. Meshkat, H. Kazemzadeh, M. Moradi, R. Bahrami, et R. Pouriamanesh, « Preparation of Graphene Nanolayers through Surfactant-assisted Pure Shear Milling Method », J. Compos. Compd

[16] Phuong Nguyen-Tri, Tuan Anh Nguyen, Pascal Carriere, and Cuong Ngo Xuan, *Hanoi, Vietnam,* 2018

[17] P. Goodhew, « General Introduction to Transmission Electron Microscopy (TEM) », in Aberration-Corrected Analytical Transmission Electron Microscopy, R. Brydson, Éd. Chichester, UK: John Wiley & Sons, Ltd, 2011

 [18] K. Akhtar, S. A. Khan, S. B. Khan, ET A. M. Asiri, « Scanning Electron Microscopy: Principle and Applications in Nanomaterials Characterization », in Handbook of Materials Characterization, S. K. Sharma, Éd. Cham: Springer International Publishing, 2018.

[19]S. Orlowska, « CONCEPTION ET PREDICTION DES CARACTERISTIQUES DIELECTRIQUES DES MATERIAUX COMPOSITES A DEUX ET TROIS PHASES PAR LA MODELISATION ET LA VALIDATION EXPERIMENTALE »

[20]K. C. Yaw, « Measurement of Dielectric Material Properties »

[21]F. Costa, M. Borgese, M. Degiorgi, et A. Monorchio, « Electromagnetic Characterization of Materials by Using Transmission/Reflection (T/R) Devices », *Electronics* nov.2017

[22]Gabriel Cormier, GELE5222 Chapitre2: Propagation d'ondes, Université de Moncton, 2012

[23] Gabriel Cormier, GELE5222 Chapitre1: Propagation d'ondes, Université de Moncton, 2012

[24] Dick Anderson, Lee Smith, Jeff Gruszynski, S-Parameter Techniques, 3000 Hanover Street, Palo Alto California, USA, 1997

Annex A

The following data shows the recorded information around the main diffraction peaks given by the XRD diffractometer.

Sample Name Cobalt	Left Angle 2-Theta °	Right Angle 2-Theta °	Left Int. Cps	Right Int Cps	Obs. Max 2-Theta °	d (Obs. Max) Angstrom
C:\DIFFDAT1'	41,14	42,26	0,82	0,93	41,679	2,16527
C:\DIFFDAT1'	46,8	48,38	2,21	1,74	47,481	1,91333
C:\DIFFDAT1'	75,44	76,64	1,41	0,57	75,997	1,25122
C:\DIFFDAT1'	83,88	84,68	0,97	0,56	84,195	1,14902
C:\DIFFDAT1'	43,62	45,12	1,19	1,34	44,377	2,03967
C:\DIFFDAT1'	51,1	52,04	1,4	1,13	51,599	1,76989
C:\DIFFDAT1'	91,6	92,88	0,96	1,28	92,335	1,08783

Sample Name Fer	Left Angle 2-Theta °	Right Angle 2-Theta °	Left Int. Cps	Right Int. Cps	Obs. Max 2-Theta °	d (Obs. Max) Angstrom
C:\DIFFDAT1'	44,48	45,34	0,34	1,23	44,838	2,01977
C:\DIFFDAT1'	64,74	65,74	0,76	0,63	65,186	1,43001
C:\DIFFDAT1'	82,02	83,2	0,64	0,92	82,5	1,16828

Sample Name FeCo br 2h	Left Angle 2-Theta °	Right Angle 2-Theta °	Left Int. Cps	Right Int. Cps	Obs. Max 2-Theta °	d (Obs. Max) Angstrom
C:\DIFFDAT1'	43,98	46,06	1,11	0,93	44,933	2,01574
C:\DIFFDAT1'	65,14	66,9	1,26	1,32	65,859	1,41703
C:\DIFFDAT1'	82,16	83,36	1,43	2,03	82,55	1,16769

Sample Name FeCo br8h	Left Angle 2-Theta °	Right Angle 2-Theta °	Left Int. Cps	Right Int. Cps	Obs. Max 2-Theta °	d (Obs. Max) Angstrom
C:\DIFFDAT1'	43,46	46	1,73	1,38	44,818	2,02062
C:\DIFFDAT1'	81,58	83,08	1,6	2,73	82,415	1,16926

Sample Name FeCo br 12h	Left Angle 2-Theta °	Right Angle 2-Theta °	Left Int. Cps	Right Int. Cps	Obs. Max 2-Theta °	d (Obs. Max) Angstrom
C:\DIFFDAT1'	43,56	46,1	2,06	2,24	44,753	2,02343
C:\DIFFDAT1'	64,34	65,76	1,73	2,42	64,914	1,43534
C:\DIFFDAT1'	81,78	83,28	1,78	2,68	82,216	1,17159

Sample Name FeCo br 36h	Left Angle 2-Theta °	Right Angle 2-Theta °	Left Int. Cps	Right Int. Cps	Obs. Max 2-Theta °	d (Obs. Max) Angstrom
C:\DIFFDAT1'	43,4	45,7	2,06	2,73	44,84	2,02828
C:\DIFFDAT1'	82,24	83,44	2,35	1,65	82,721	1,16572
C:\DIFFDAT1'	81,06	82,4	1,84	2,42	82,056	1,17345
C:\DIFFDAT1'	64,42	66	1,88	1,48	65,034	1,45287

Sample Name FeCo br 60h	Left Angle 2-Theta °	Right Angle 2-Theta °	Left Int. Cps	Right Int. Cps	Obs. Max 2-Theta °	d (Obs. Max) Angstrom
C:\DIFFDAT1'	43,4	46,26	2,85	2,32	44,66	2,00742
C:\DIFFDAT1'	64,66	65,76	1,68	2,07	65,071	1,45226
C:\DIFFDAT1'	81,84	82,88	3,68	3,71	82,351	1,17001